Ph.D. Dissertation of Natural Sciences

Degradation of Scene-dependent Rate Modulation of the CA3 Place Cells in the Absence of the Dentate Gyrus Inputs during Ambiguous Scene Retrieval

치상회 손상에 따른 CA3 장소세포의
장면의존적 발화율 변조의 저하

August 2020

Graduate School of Natural Sciences
Seoul National University
Brain and Cognitive Sciences Major

Choong-Hee Lee

Abstract

The ability to differentiate similar experiences into discrete events in memory is a fundamental component of the episodic memory. Computational models and experimental evidence have suggested that projections from the dentate gyrus (DG) to CA3 play important roles in representing orthogonal information (i.e., pattern separation) in the hippocampus. However, the effects of eliminating the DG on neural firing patterns in the CA3 have rarely been tested in a goal-directed memory task that requires both the DG and CA3. In this thesis, the simultaneous application of lesion and in-vivo electrophysiology were used to examine the role of the DG inputs to the CA3 as the animal processes scene memory. Selective lesions in the DG were made using colchicine in male Long-Evans rats, and CA3 single units were recorded as the rats performed visual scene memory tasks. The original scenes used in training were modified during testing by blurring to varying degrees, by using visual masks, or by overlaying competing scenes to examine how changes in scenes differentially recruit the DG-CA3 circuits. Compared with controls, the performance of rats with DG lesions was particularly impaired when blurred scenes were used in the task. The firing-rate modulation associated with visual scenes in these rats was significantly reduced

in the single units recorded from the CA3 when blurred scenes were presented, largely because DG-deprived CA3 cells did not show stepwise, categorical rate changes across varying degrees of scene ambiguity compared with controls. These findings suggest that the DG plays key roles not only during the acquisition of scene memories but also when modified visual scenes are processed in conjunction with the CA3 by making the CA3 network respond orthogonally to ambiguous scenes.

Keywords: hippocampus, dentate gyrus, CA3, place cell, pattern separation, rate modulation

Student Number: 2011-24035

Table of Contents

List of Figures

List of Tables

Background

1. Scene and the hippocampus

The hippocampus plays an essential role in remembering events as discrete memories (Eichenbaum, 2000). The first study to report the functional significance of the hippocampus was based on a case study centering on a human patient, Henry Gustav Molaison, who underwent a bilateral medial temporal lobectomy (Scoville and Milner, 1957). The surgical removal of the bilateral medial temporal lobe, which included the hippocampus, have caused specific mnemonic impairments. The patient suffered from anterograde amnesia and partial retrograde amnesia but was spared with motor skill learning. This finding has led many neuroscientists to further investigate the role of the hippocampus in episodic memory, as well as organizing different types of memory systems (Squire and Zola-Morgan, 1991).

Endel Tulving's definition of episodic memory is the memory of an event or series of events that comprise an episode (Tulving et al., 1972). The mental representation of such memory would contain "what", "where" and "when" information, which led to using associative learning tasks to investigate how episodic memory is formed in the brain. In humans, incidental association tasks have been used to identify what brain regions were activated when successful source memory was retrieved in the later testing sessions

(Brewer et al., 1998; Davachi et al., 2003; Stark and Okado, 2003; Kirwan et al., 2008). In rodent and nonhuman primate studies, ‘episodic-like’ memory tasks have been used to examine what brain regions are essential for learning the association and how it is represented in the brain on the neuronal level(Murray and Mishkin, 1998; Aggleton and Brown, 1999; Dudchenko et al., 2000; Eacott and Norman, 2004; Fortin et al., 2004).

The other important function of the hippocampus is its role in spatial memory. In 1971, O’Keefe and Dostrovsky found the place cells in the hippocampus, which are neurons that show highly selective firing based on the location of the animal (O'Keefe and Dostrovsky, 1971). The discovery of the place cells has shown that the hippocampus has an internal representation of the environment and provided solid support for the cognitive map theory (O'Keefe and Nadel, 1978). Further studies have reported that the spatial firing of the place cells was modulated by visual changes in the surrounding environment and that the place cells may be critical for mnemonic information processing of the hippocampus (O'Keefe and Conway, 1978; Muller and Kubie, 1987; Lee et al., 2004a; Delcasso et al., 2014).

Gaffan was one of the first to suggest that the scene memory could be the basis of the episodic memory (Gaffan, 1991, 1994). A scene can be defined as a set of visual stimuli that convey a semantically coherent view of the environment, composed of background elements and objects in a specific spatial layout

(Henderson and Hollingworth, 1999). A scene represents a space in which objects or actors move and make events. Therefore, the ability to process scenes could be a major component needed for both episodic memory and spatial memory.

Literature in both humans and animals is consistent with the notion that the hippocampus is important for scene processing. Human patient studies have suggested that the damages to the hippocampus disrupted the ability to process or construct scenes (Hassabis et al., 2007; Mullally et al., 2014). Neuroimaging studies have further supported the idea by reporting that the activity patterns in the human hippocampus are modulated when scene processing is required (Bonnici et al., 2012; Brown et al., 2014; Zeidman et al., 2015). In rodents, perturbation studies have shown that functioning hippocampus is required in scene-dependent spatial choice tasks (Lee and Solivan, 2010; Kim et al., 2012; Lee et al., 2014). Electrophysiological recording of the hippocampal CA1 single-units has shown scene-dependent firing rate modulations during the same task (Delcasso et al., 2014).

2. Anatomical properties of hippocampal subregions and their proposed roles

Distinct anatomical characteristics of the hippocampus that differs from the neocortex have captured the attention of neuroanatomists from the earlier era of the neuroscience. Contrary to the reciprocal projections commonly found in the neocortex (Felleman and Van Essen, 1991), the connection between hippocampal subregions are mostly unidirectional (Ramón y Cajal, 1893; de No, 1934). The hippocampal formation refers to brain regions that are part of these feedforward connections and is composed of the dentate gyrus, the hippocampus proper, the subicular complex, and the entorhinal cortex (Amaral and Witter, 1989). The term “trisynaptic circuit” is used to define three excitatory projections within the hippocampal formation that has been the center of focus. It refers to the connection originating from the entorhinal cortex to DG which projects to CA3, which projects to CA1 (Andersen et al., 1969).

The dentate gyrus mostly receives its input from layer II of the entorhinal cortex, which is named the perforant pathway (Ramón y Cajal, 1893). The inputs from the entorhinal cortex via perforant path fibers mostly innervate granule cells (Claiborne et al., 1990), which are principal neurons located in the molecular layer of the dentate gyrus. The number of granule cells is six times much larger than that of other hippocampal subregions (Boss et al., 1985; Amaral et al., 1990). Granule cells are also known for their sparse activity, which

is supported by the local inhibitory network (Barnes et al., 1990).

CA3 receives its input from three regions: dentate gyrus, entorhinal cortex, and CA3 itself. The projection from the dentate granule cells to the CA3 pyramidal cells is called the mossy fiber pathway (Amaral et al., 2007). CA3 also receives projections from the entorhinal cortex via the perforant pathway, as well as from CA3 itself via recurrent collaterals (Gonzales et al., 2001). Compared to diffuse projections from the entorhinal cortex or CA3, CA3 neurons only receive sparse and topographic projections from the mossy fiber pathway (Claiborne et al., 1986). Due to its proximity to soma, the mossy fiber inputs are known to have larger synapses and suggested to be stronger compared to other inputs (Brown and Johnston, 1983).

Based on the anatomical connections within the hippocampus, computational models have suggested that the hippocampus supports forming and retrieving distinct memory representations by providing two key processes: pattern separation and completion (Marr, 1971; O'Reilly and McClelland, 1994; Rolls and Kesner, 2006). Pattern separation consists of the formation of orthogonal representations despite similar input patterns, whereas pattern completion consists of the retrieval of original memory representations when presented with modified or ambiguous stimuli.

Computational models have suggested that different subregions of the hippocampus are responsible for pattern separation and completion processes (O'Reilly and McClelland, 1994; Treves and Rolls, 1994; Kesner and Rolls, 2015). Specifically, some

computational models have emphasized that the dentate gyrus (DG) subregion in the hippocampus is critical in the formation of orthogonal representations of events and places in the CA3, the hippocampal structure downstream of the DG. The CA3 is important in recovering the original memory representation (i.e., pattern completion) when slightly modified inputs are fed from the cortical areas, mainly due to the recurrent network component in the CA3. To have orthogonalized representations in the CA3 despite its auto-associative network properties, CA3 neurons require sparse, but strong inputs from the DG. It has been hypothesized that two seemingly opposite computational processes performed in the hippocampus are critical in classifying a current environment based on prior original experience.

3. Physiological evidence for pattern separation in the hippocampus

Consistent with the computational models, experimental evidence using rodents has provided support for these computational models (McNaughton et al., 1989; Gilbert et al., 1998; Gilbert et al., 2001; Lee and Kesner, 2004; Lee et al., 2004a; Lee et al., 2004b; Leutgeb et al., 2004; Lee and Solivan, 2010; Neunuebel and Knierim, 2014; Lee et al., 2015; van Dijk and Fenton, 2018). For example, behavioral studies using rats with lesions in the DG found significant impairment in memory retrieval when performing tasks requiring the differentiation of similar locations (Gilbert et al., 2001) or similar object-place paired associates (Lee and Solivan, 2010). We recently reported that DG lesions impair the acquisition of new visual scenes and that rats with DG lesions were deficient in recognizing visual scenes when the original scenes were altered to make them ambiguous (Ahn and Lee, 2014). These findings indicate that DG is important for disambiguating similar experiences.

Studies using human subjects have also reported the roles of the hippocampus in pattern separation (Kirwan and Stark, 2007; Bakker et al., 2008; Brown et al., 2010; Lacy et al., 2011; Motley and Kirwan, 2012; Berron et al., 2016). These studies have employed a task called “mnemonic similarity task (MST)”, in which participants had to respond differently to the novel, repeated, and lure images. The increased activity when the participant viewed ‘lure’ images, in

which a minor component within the image has changed, compared to repeated images were observed around the dentate gyrus. However, these studies provide limited information since the distinction between the DG and CA3 is difficult to make using the current fMRI techniques. These technical challenges also apply to the electrophysiology characterization of the DG/CA3 areas in pattern separation in nonhuman primates (Sakon and Suzuki, 2019).

4. Limitations of past electrophysiological studies in examining the role of the dentate gyrus in pattern separation

Physiologically, very few granule cells are active during behavior in the DG and those active ones tend to fire only in a single environment (Danielson et al., 2017; GoodSmith et al., 2017; Senzai and Buzsaki, 2017), suggesting their roles in pattern separation (Nakazawa, 2017). Despite the behavioral and physiological evidence supporting the role of the dentate gyrus in pattern separation in the hippocampus, the underlying neural mechanisms are largely unknown. In contrast, electrophysiological studies of the CA3 have yielded evidence for both pattern separation (Leutgeb et al., 2007) and pattern completion (Lee et al., 2004b; Neunuebel and Knierim, 2014). Heterogeneity may be present along the transverse axis of the CA3, with the proximal and distal CA3 specialized for pattern separation and pattern completion, respectively (Lee et al., 2015).

Fenton and his colleagues have reported that optogenetic inhibition of dentate granule cells caused behavioral impairment in the place avoidance task only when there was a conflicting memory (van Dijk and Fenton, 2018). Despite the spatial remapping observed in DG place cells in response to spatial cue modifications, the authors did not find any changes in spatial firing patterns in the DG granule cells that reflected the memory discrimination. Leutgeb group has reported that colchicine-induced DG lesions caused impaired

performance in the spatial working memory task on the radial arm maze (Sasaki et al., 2018). In addition, CA3 units with DG lesion showed reduced spatial selectivity, as well as reduced occurrence of sharp-wave ripple (SWR) events near the goal locations.

Recently, literature has focused on more specific components within the dentate gyrus, such as mossy cells or adult neurogenesis. Knierim and his colleagues have used a juxtacellular recording technique to dissociate the activities of granule cells, mossy cells, and CA3 pyramidal cells (GoodSmith et al., 2017). In this study, the rats performed foraging tasks on different mazes while the authors recorded spatial firing patterns in these three types of neurons. The result shows that the granule cells and CA3 pyramidal cells showed place fields in mostly one or none of the mazes, while the mossy cells showed multiple place fields across different mazes. In a study by Senzai and Buzsaki, the sparse firing characteristics of the granule cells and multiple place fields in the mossy cells were similarly reported (Senzai and Buzsaki, 2017). In this study, the place fields of the dentate granule cells were more stable across different mazes compared to the mossy cells or CA3 pyramidal cells, which conflicts with the results from the Knierim's group, where granule cells' place fields often appeared in only one of the mazes. The importance of the mossy cells is well supported by another study by Nakazawa and his colleagues (Jinde et al., 2012). This study reported that the selective ablation of mossy cells resulted in hyper-excitability of DG granule cells and caused impaired behavior in the contextual fear

conditioning task in which the mice had to discriminate two contexts.

Most previous physiological studies, however, were conducted using behavioral paradigms that did not require rats to use such computational processes to guide their behavior (GoodSmith et al., 2017; Senzai and Buzsaki, 2017). Although physiological recordings were made after the DG became dysfunctional in mnemonic tasks in some studies, there was a lack of control over stimulus ambiguity (McNaughton et al., 1989; Jinde et al., 2012; Sasaki et al., 2018; van Dijk and Fenton, 2018). More importantly, these studies did not characterize the changes in neural activity in the CA3 that resulted from the absence of the DG network.

Chapter 1. Recognition of ambiguous visual scenes following the lesion of the dentate gyrus

Introduction

The hippocampus is important for visual scene memory. Previous studies in our laboratory have shown that the inactivation of the dorsal hippocampus results in impaired performance in the visual scene memory tasks (Kim et al., 2012; Delcasso et al., 2014; Lee et al., 2019). Based on the anatomical characteristics of the dentate gyrus, theoretical models have suggested that the DG-CA3 circuit is important for storing similar, but different experiences into orthogonalized representations (O'Reilly and McClelland, 1994; Treves and Rolls, 1994). Behavioral and physiological studies have consistently supported that the dentate gyrus is important for encoding (Rolls and Kesner, 2016). However, the role of the dentate gyrus in the retrieval process has been overlooked, specifically when there are alterations in the well-learned stimuli.

In this study, the effects of the selective lesion to the dentate gyrus are examined while rats performed visual scene memory (VSM) tasks. The scene stimuli used in the VSM tasks were manipulated to increase ambiguity in various manners to investigate the role of the dentate gyrus in the retrieval of well-learned scene memory from degraded inputs.

Materials and methods

Subjects

Eight male rats (Long-Evans) weighing 300–400 g were used. Food was restricted to maintain the body weight at 85% of free-feeding weight, and water was available ad libitum. All animals were individually housed with a 12 h light/dark cycle. All animal protocols were approved by the Institutional Animal Care and Use Committee of Seoul National University.

Behavioral apparatus

The behavioral task was conducted on an elevated, T-shaped linear track (73 x 8 cm stem with two 38 x 8 cm arms), containing a food well (2.5 cm diameter, 0.8 cm deep) at the end of each arm (Fig. 1). Each food well was covered by a black, acrylic washer with a silver reflective sticker attached on the bottom surface to record the moment the rat displaced the washer to access the reward with an optic sensor (Autonics) attached to the center of the food well. One of the food wells was baited during the intertrial interval while the rat was confined in a start box. To prevent the rat from locating the baited food well by possible unintended auditory cues from manipulating the washer on the corresponding side, both washers were adjusted equally during the procedure. A guillotine door-operated start box (22.5 x 16 x 31.5 cm) was attached to the side opposite to the stem. Three LCD monitors displaying visual scene

stimuli were installed to surround the arm portions of the T-shaped track. Four optic fiber sensors were inserted along the track at distances from the start-box door of 1, 27, 47, and 67 cm to detect the position of the animal and to control the onset and offset of the scenes. Sensor signals were sent to a data-acquisition system (Digital Lynx SX, Neuralynx) as transistor-transistor logic (TTL) signals. Custom-written software created in MATLAB (MathWorks) and Psychtoolbox was used to control scene stimuli and transmit TTL signals containing trial information to the data-acquisition system. During the task, the experimental room was dimly lit with an array of dim LEDs. A camera was attached to the ceiling to record the rat's position and head direction at a sampling rate of 30 Hz. The apparatus was surrounded with a black curtain, and white noise was played by two speakers (80 dB) during behavioral sessions to mask unwanted environmental noises.

Figure 1. Behavioral apparatus for the visual scene memory task. The apparatus is based on a T-maze. In each trial, the door on the start box (grey box in the bottom) was manually opened, which were detected by one of the four optic sensors. The scene stimuli were presented on three LCD monitors immediately after opening the start box door. Rats were trained to make a spatial choice toward either left or right arm, depending on the scene presented. Each arm had a food well covered with a black acrylic washer. Pushing the washer aside was detected by optic sensors attached beneath the well.

Visual scene memory task

A visual scene memory (VSM) task previously used to show that rats with DG lesions were impaired in the acquisition of visual scene memory and the retrieval of ambiguous scenes was used in the present study (Ahn and Lee, 2014). A trial was started by opening the door of the start box. This opening was detected by the optical sensor, which immediately triggered the presentation of the visual scenes on the monitors. The rat ran along the track to the end of the stem and had to choose either the left or right arm, depending on the visual scene, to obtain food reward (Fig. 1). A food well was placed at the end of each arm and covered with a black acrylic disk to prevent the animal from using odor to sense a reward. A quarter piece of cereal (Froot-Loops, Kellogg's) was hidden in the food well in the arm that was correctly associated with the scene; the rat retrieved the hidden reward by pushing aside the black acrylic disk. If the rat chose incorrectly, no reward was provided, and the rat was gently guided back to the start box immediately after making the incorrect choice. The intertrial intervals (ITIs) following correct and incorrect choices were set at 10 s and 20 s, respectively.

During each ITI, a reward for the next trial was placed in one of the food wells while the rat was confined to the start box. Four grayscale visual patterns (zebra, pebbles, bamboo, and mountains) were used as scene stimuli. The luminance of the visual scenes was equalized to an average intensity of 103 in Adobe Photoshop. Zebra and bamboo scenes were associated with the left food well, whereas

pebbles and mountain scenes were associated with the right food well (Fig. 2). Rats were trained to criterion (70% correct choice for each scene on two consecutive days), initially with a pair of visual scenes and subsequently with a second pair of scenes. Training sessions before surgery consisted of 40 trials. The presentation sequence for scenes in a given session was pseudorandomized so that (1) each scene was presented an equal number of times in every 20 trials, and (2) the same food well was not used for reward during four consecutive trials. Surgery was performed once the rats had learned both pairs of scene stimuli to criterion.

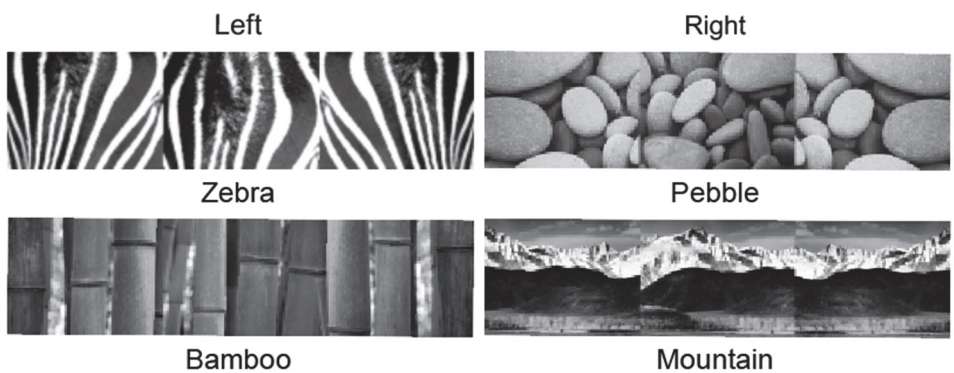

Figure 2. Original four visual scenes used in the VSM task. During the pre-surgical training, zebra and pebble scenes used first as a pair. Once performance reached criterion, the second pair of scenes (bamboo and mountain) were used. Zebra and bamboo scenes were associated with the left arm, and pebble or mountain scenes were associated with the right arm.

Surgery

Rats trained to criterion were randomly assigned to the lesion group or the control group. Rats were placed under deep anesthesia by intraperitoneal injection of sodium pentobarbital (Nembutal, 65 mg/kg), and their heads were fixed in a stereotaxic frame (Kopf Instruments, Tujunga, CA). Anesthesia was maintained with 0.5–2% isoflurane mixed with 100% O2 throughout the surgery. An incision was made along the midline of the scalp to expose the skull. The stereotaxic adapters were adjusted to place the bregma and lambda on the same horizontal plane. Four small burr holes and one big burr hole were drilled. The small burr holes were used for injection and the large holes for hyperdrive implantation. Either colchicine (7 mg/mL, 0.2 μL/site at 10 mL/h) or saline (0.2 μL/site at 10 mL/h) was injected into the dorsal DG at the following coordinates: 1) 2.8 mm posterior to the bregma, ±1.1 mm lateral to the midline, and 3.7 mm ventral from the dura, and 2) 4.0 mm posterior to the bregma, ±2.3 mm lateral to the midline and 3.2 mm ventral from the dura.

Colchicine is a neurotoxin that, when injected into the hippocampus, selectively ablates granule cells in the DG, while having a minimal effect on the principal cell layers in the CA1 and CA3 (Walsh et al., 1986; Xavier et al., 1999). Colchicine or saline was injected using a custom-made 10 μL glass pipette (Marienfeld, Germany) with tips at least 8 mm long to minimize damage to the overlying cortical regions. At each site, the glass pipette was maintained at the injection depth for 2 minutes after infusion to avoid

the possible upward spread of colchicine. Control animals underwent the same surgical procedures except that artificial cerebrospinal fluid (aCSF) was injected into the DG. All injections were made by connecting a 10 mL Hamilton syringe operated with a microinjection pump (Cole-Parmer, Vernon Hills, IL).

Once injections were finished, a hyperdrive carrying 24 tetrodes and three reference electrodes was implanted into each rat to record spikes from single units in the dorsal CA3. The impedance of each tetrode was adjusted to 100–300 kOhm (measured in gold solution at 1 kHz with an impedance tester) 2 days before surgery. The surgical coordinates for making the large burr hole was predetermined to allow the tetrodes to cover a range 2.5–5 mm posterior to the bregma and 2.5–5 mm lateral to the midline. The hyperdrive was affixed to the skull by applying bone cement to its bundle and multiple skull screws around the bundle. After surgery, rats were orally administered diluted ibuprofen syrup to attenuate pain and cared for in a veterinary intensive care unit for 24 hr. The details of these surgical procedures have been described previously (Ahn and Lee, 2014; Delcasso et al., 2014).

The behavioral paradigm for recording sessions

Once the electrophysiological recording session began, all four scenes shown during the training period were presented in a pseudorandomized order in a testing session of familiar scenes (Familiar, ~160 trials per session) (Fig. 2). Once rats performed well

in familiar sessions for two consecutive days, they were subjected to a blurred version of the task (*Blurred*). Each *Blurred* session began with 10 trials of an unaltered pair of scenes (zebra and pebble scenes on the first day, and bamboo and mountain scenes on the second day), followed by a presentation of modified versions of the original pair of scenes (30%, 40%, 50% and 70% Gaussian blurred images) along with the original scenes (~160 trials per session) (Fig. 3A). After two days of *Blurred* sessions, rats were subjected to *Overlay* sessions for two days, followed by a *Masked* session. Procedures for the *Overlay* and *Masked* sessions were identical to those of the *Blurred* sessions, except that visual scene stimuli were altered differently. For the *Overlay* sessions, two scene stimuli with different opacity values were mixed to create a single visual scene (Fig. 3C, bottom). In the *Masked* sessions, Gaussian blurred images were replaced by partially occluded images with visual masks composed of viewing holes of four different diameters (Fig. 3B, middle). This manipulation was intended to create partial cues that may require pattern completion. Once the *Masked* sessions were completed, rats were subjected to a session with novel scenes for two days. The results of the Novel scene sessions are not included in the current study.

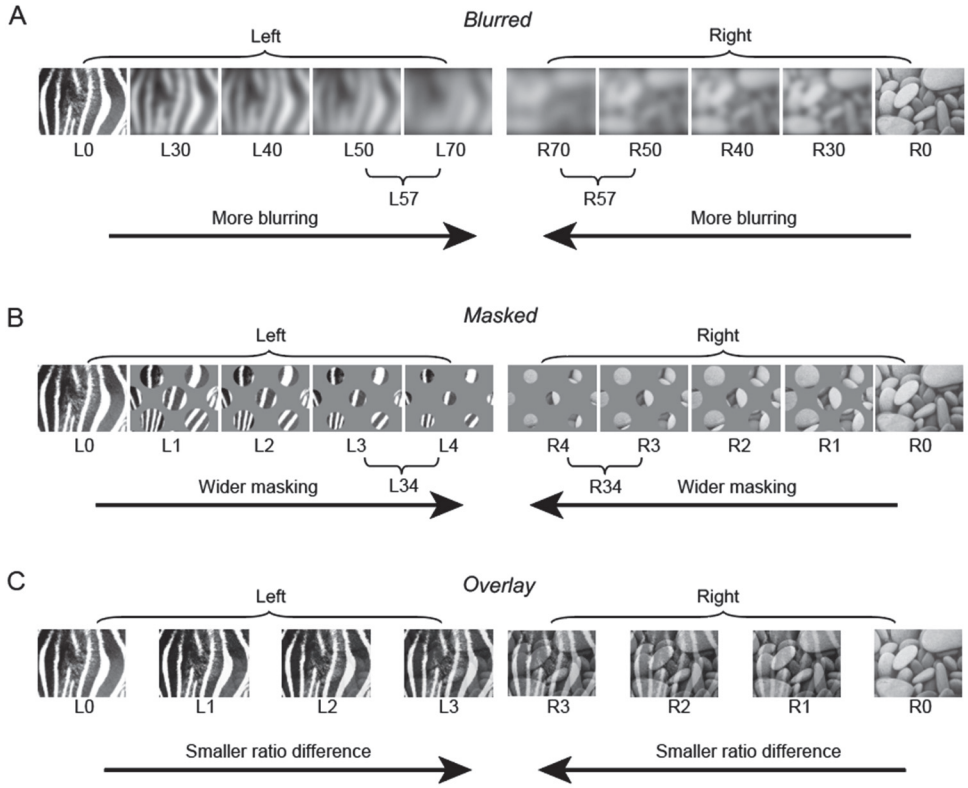

Figure 3. Altered scenes used in the VSM task. (A) In the *Blurred* condition, original scenes were applied with different levels of Gaussian smoothing. (B) In the *Masked* condition, original scenes were masked with different sizes of circular openings. (C) In the *Overlay* condition, paired scenes (zebra and pebble, bamboo, and mountain) were overlaid on each other with different degrees of opacity.

Histology

Once all recording sessions were concluded, the rats were subjected to histological procedures to assess the extent of the neurotoxic lesions and to determine the locations of the tetrodes. Rats were administered an inhaled overdose of CO2 and transcardially perfused with a solution of 4% (v/v) formaldehyde in 0.1 M PBS. Their brains were extracted and stored in a 30% sucrose-formalin solution until they were fully submerged. Each brain was gelatin-coated, again soaked in 30% sucrose-formalin solution, and sectioned at 40 μm depth using a freezing microtome (HM 430, ThermoFisher Scientific). The brain sections were mounted and stained with thionin, and photomicrographs of these sections taken with a digital camera (Eclipse 80i, Nikon) attached to a microscope at x1 magnification. Brains were reconstructed from these sections to match the configuration of the tetrodes of the pre-surgical bundle design. The exact locations of tetrodes were determined using the 3D reconstructed images and physiological depth profiles recorded during the tetrode adjustment period. To examine the integrity of cell layers in the DG and CA3, additional photomicrographs of the brain sections were taken with a digital slide scanner (MoticEasyScan, Motic) at x40 magnification.

Volumetry

To evaluate the effect of colchicine infusion, we conducted a 3D volumetric analysis (Lee et al., 1999; Ahn and Lee, 2014) for

hippocampal subregions: CA1, CA3, and DG. Among the thionin-stained brain sections acquired, 18 brain sections from 2 to 4 mm posterior to the bregma were used for the volumetric analysis. In each section, principal cell layers were traced with a color corresponding to one of the hippocampal subregions. For each subregion, we calculated the percent voxel index of individual rats, in which the mean of the number of colored pixels from four control rats was set as 100% (ImageJ, NIH). For statistical comparison, we performed a two-way ANOVA with group and subregion as factors, implemented in JMP 11 statistical software package (SAS Institute, Cary, NC). The results of post-hoc t-tests comparing groups and subregions were corrected using a Bonferroni correction procedure for multiple comparison corrections. To ensure that the recording locations between the control and DG-lesion groups were homogeneous, we calculated the relative position of each tetrode by measuring the length of the CA3 layer. The relative position of zero denotes the most proximal CA3, whereas 1 denotes the boundary between CA3 and CA2 pyramidal layers.

Data analysis

Experimental design and statistical analysis

Behavioral performance from all recording sessions (Familiar, *Blurred*, *Overlay*, *Masked*, and Novel) was analyzed using a three-way repeated-measures ANOVA (group, session type, and day) with the rat identity nested within the group factor, implemented in JMP

11 statistical software package (SAS Institute, Cary, NC). The results of post-hoc t-tests for ANOVA tests (Fig. 4) comparing session type and group were corrected using a Bonferroni correction procedure for multiple comparison corrections. For the *Blurred*, *Overlay,* and *Masked* sessions, a two-way repeated-measures ANOVA (group, ambiguity level) with the rat identity nested within the group factor was used (Fig. 5). The post-hoc t-tests for comparing ambiguity levels and groups were corrected using Bonferroni correction procedures for multiple comparisons.

Results

Lesions in the DG impair the ability of rats to disambiguate visual scenes

Four rats each in the control group and DG lesion groups were first tested with unaltered, familiar visual scenes (Fig. 2), followed by the *Blurred*, *Overlay* and *Masked* sessions (Fig. 3). Compared with controls, DG lesions affected performance differently, depending on the type of stimulus manipulations. Three-way repeated-measures ANOVA, with group, session type and day as factors, revealed a significant main effect of session type ($F_{(4, 53.08)} = 11.045$, $p = 0.001$) and significant interaction between group and session type ($F_{(4, 53.08)} = 4.16$, $p = 0.005$). The main effect for group ($F_{(1, 12.21)} = 3.61$, $p = 0.081$) or day ($F_{(1, 53.17)} = 0.038$, $p = 0.845$) and interaction between group and day ($F_{(1, 53.17)} = 0.174$, $p = 0.678$), session and day ($F_{(4, 53.17)} = 2.49$, $p = 0.054$), and the three-way interaction ($F_{(4, 53.17)} = 1.66$, $p = 0.173$) were not significant. When the original scenes were used as stimuli in the Familiar session, the control and DG-lesion groups performed similarly, around 90% ($t_{(53.27)} = 0.09$, $p = 0.249$, Bonferroni-corrected, Familiar in Fig. 4). However, when visual scenes were made ambiguous in the *Blurred* session, rats with DG lesions showed a significant reduction in response accuracy compared with controls ($t_{(53.27)} = -2.68$, $p = 0.01$, Bonferroni-corrected post-hoc t-test, *Blurred* in Fig. 4). In the *Masked* sessions, both groups showed about 85% accurate responses, with no

significant difference between the control and DG-lesion groups ($t_{(53.27)}$ = -1.42, p = 0.35, Bonferroni-corrected post-hoc t-test, *Masked* in Fig. 4). Similarly, behavioral performances were similar between two groups during the *Overlay* sessions ($t_{(53.27)}$ = 1.65, p = 0.10, Bonferroni-corrected post-hoc t-test, *Overlay* in Fig. 4).

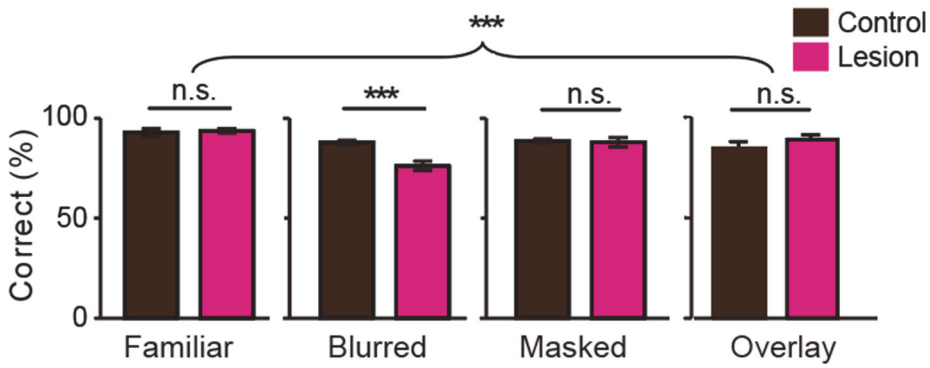

Figure 4. Behavioral performance in the VSM task. The behavioral performance of the two groups under different scene conditions is shown. Mean ± standard error. ***p < 0.001.

The accuracy of choices made by the control and DG-lesion groups across different ambiguity levels during the *Blurred*, *Masked* and *Overlay* sessions were compared by two-way repeated-measures ANOVA, with group and ambiguity level as factors. In the *Blurred* session, the results showed a significant interaction between group and ambiguity level ($F_{(4,64)}$ = 3.901, p = 0.006). Compared with control rats, rats with DG lesions showed significant impairment in response accuracy at ambiguity levels ≥ 40 ($t_{(68)}$ = -2.22, p = 0.015, $t_{(68)}$ = -3.87, p = 0.0001 and $t_{(68)}$ = -3.38, p = 0.001, respectively for 40, 50 and 70 conditions, Bonferroni-corrected post-hoc t-test, Fig. 5A), but not at ambiguity levels < 40 ($t_{(68)}$ = 0.35, p = 0.723 and $t_{(68)}$ = -0.58, p = 0.28, respectively for 0 and 30 conditions, Bonferroni-corrected post-hoc t-test). However, in the *Masked* (Fig. 5B) and *Overlay* (Fig. 5C) sessions, the main effect of ambiguity level was significant (*Masked*: $F_{(4,64)}$ = 10.128, p = 0.001; *Overlay*: $F_{(3,43)}$ = 4.746, p = 0.01) with no significant group effect (*Masked*: $F_{(1,68.83)}$ = 0.013, p = 0.91; *Overlay*: $F_{(1,43.18)}$ = 0.003, p = 0.956) and no significant interaction effect as well (*Masked*: $F_{(4,64)}$ = 0.947, p = 0.442; *Overlay*: $F_{(3,43)}$ = 0.178, p = 0.911).

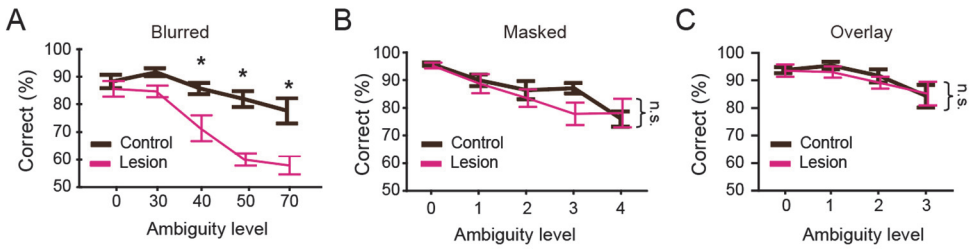

Figure 5. Behavioral performance across ambiguity levels in altered scene conditions. (A) Behavioral performance of the two groups across different ambiguity levels in *Blurred* sessions. Mean ± standard error. n.s.: not significant. *p < 0.05. (B) Same as E, but in *Masked* sessions. Mean ± standard error. (C) Same as E, but in *Overlay* sessions. Mean ± standard error.

Histological verification of colchicine-induced lesions

Injection of colchicine into the dorsal DG ablated the granule cell layer and the hilar region while leaving the CA3 pyramidal layer relatively intact (Fig. 6B). Compared to the aCSF-injected controls (Fig. 6A, effect of interaction: $F_{(2, 12)} = 91.08$, $p = 0.001$), the rats with colchicine injection showed almost complete damage (~85%, $t_{(15.88)} = -18.59$, $p = 0.001$, Bonferroni-corrected) of the DG granule cell layer (Fig. 7). CA1 subregion also showed considerable damage (~35%, $t_{(15.88)} = -6.90$, $p = 0.001$, Bonferroni-corrected), but there was no significant difference between control and lesion group in the CA3 ($t_{(15.88)} = -2.74$, $p = 0.22$, Bonferroni-corrected). The extent of the damages observed in this study was consistent with the previous reports (McNaughton et al., 1989; Lee and Kesner, 2004; Ahn and Lee, 2014; Sasaki et al., 2018).

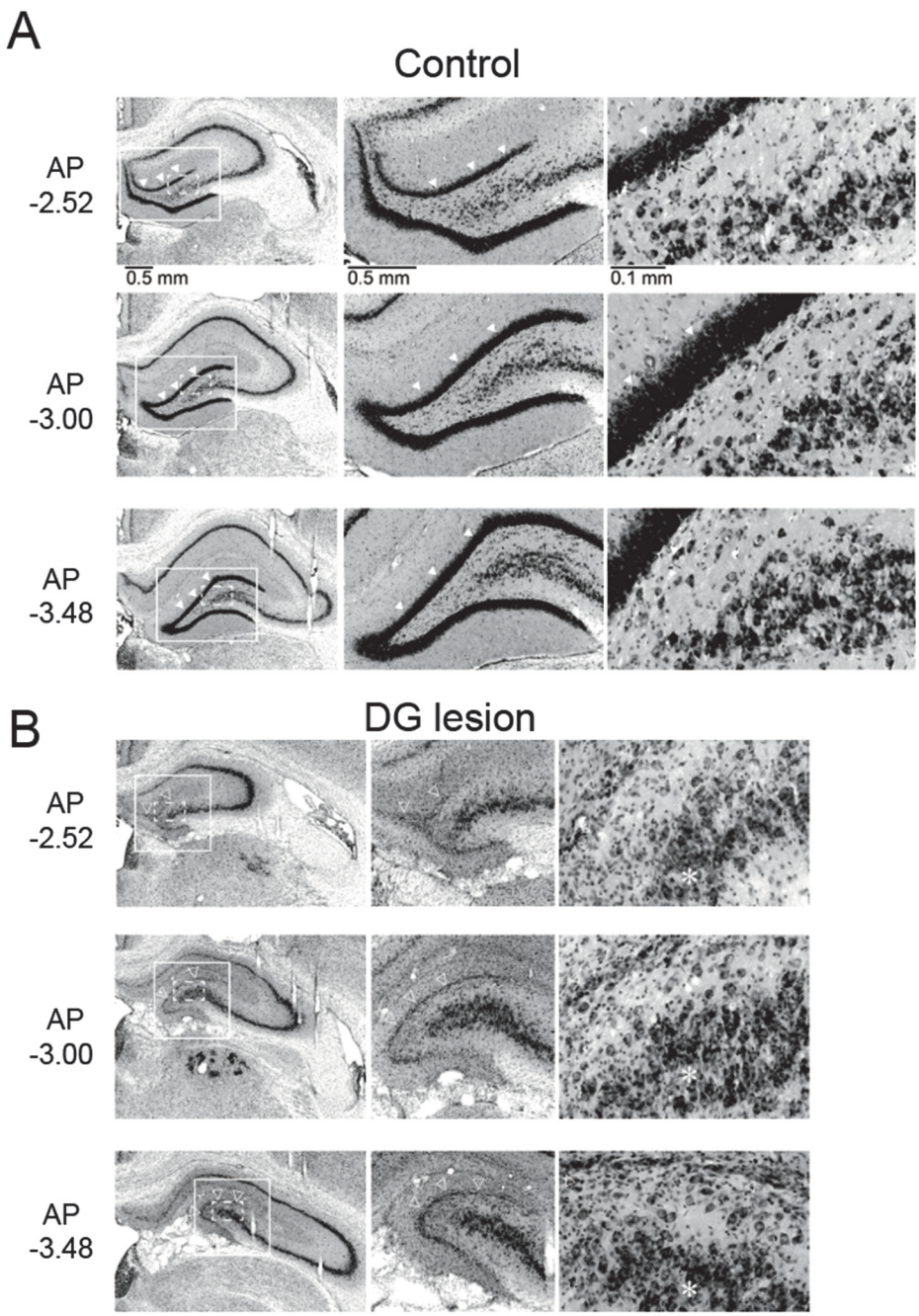

Figure 6. Histological verification of DG lesions. (A) Examples of thionin-stained sections from the control and DG-lesion groups. For each hippocampal section (4x magnification, left), the DG/hilar area (white rectangle) was zoomed and shown as

a magnified image (10x magnification, middle). The suprapyramidal blade of the DG and the hilar area (dashed white rectangle) was further zoomed to show changes observed in the DG granule cell layer and CA3 pyramidal layer (40x magnification, right). Solid and open arrowheads indicate intact and damaged granule cell layers in the control and lesion groups, respectively. Asterisks in the DG-lesion group denote the relatively intact pyramidal cell layers in the CA3. Scale bars are shown below the sections. AP coordinates (distances from bregma) are given at the left bottom corner of each section.

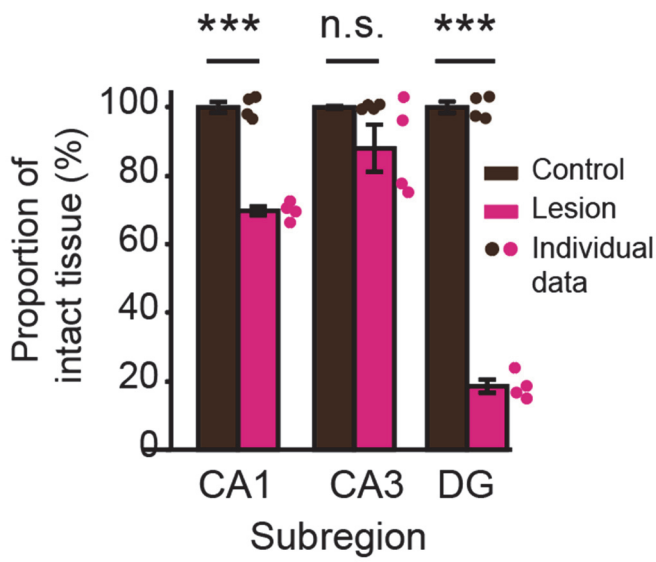

Figure 7. The extent of the lesion in the hippocampal subregions based on the 3D volumetry. Proportions of intact tissue in individual rats are shown in colored dots next to the bar graphs. Mean ± standard error. n.s.: not significant, ***$p < 0.001$.

Discussion

These findings strongly suggest that the DG plays an important role in recognizing ambiguously blurred versions of the familiar visual scenes, but not when the visual scenes are unaltered in other ways. Because the performance of the control and lesion groups did not differ significantly from each other when the visual scenes were relatively mildly blurred (i.e., 30%), it is likely that the DG lesions affected visual pattern separation when substantial noise (i.e., ≥ 40% Gaussian blur) was added to the original scene stimuli.

In the previous study from our laboratory, DG lesions have caused behavioral impairment in both retrieval of blurred scenes and the acquisition of novel scenes (Ahn and Lee, 2014). Therefore, it was possible to interpret that the DG-lesioned rats were impaired in processing any new scenes. The novelty of the behavioral findings in the current thesis is that we have shown that not any modifications to the well-learned stimuli are affected by DG lesions. This finding sheds light on the importance of the DG in the retrieval process, which was often overlooked in the hippocampal literature.

In the current study, the injection of colchicine for DG lesions also caused mild damages in the CA1 pyramidal layer. However, it is less likely that impaired performance in the *Blurred* sessions was caused by the damages to the CA1. In a previous study from Kesner's group have shown that colchicine induced lesions are different from

ibotenic acid-induced CA1 lesions (Gilbert et al., 2001). In this study, rats with DG lesion or CA3 lesion were impaired in the spatial pattern separation task, while being intact in the temporal sequence retrieval task. Conversely, rats with CA1 lesions were impaired in the temporal sequence retrieval task, but intact in the spatial pattern separation task. The dissociations found between the DG lesion and CA1 lesion groups indicate that the result of the current study was not driven by the damages to the CA1.

Interestingly, the DG-lesioned rats were also minimally affected by the overlaying of two visual scene stimuli (*Overlay* session). The overlaying visual stimuli were intended to mimic the visual object morphing conditions (Ahn and Lee, 2014). The scene overlay may have been qualitatively different from the object morphing. Visual stimuli with two scenes overlaying on each other with different opacity levels may have left structural cues for both scenes. The image analysis using the structural similarity index (Wang et al., 2004) suggested that overlaid or masked scene stimuli were more similar to the original images compared to blurred scene stimuli. The difference in task difficulty may have driven different impairment patterns observed between the Blurred sessions and the other two session types. However, degraded structural components in the blurred scene stimuli alone cannot explain the impairment patterns observed in the *Blurred* sessions. Based on the structural similarity index, the blurred scene stimuli (L30~70 or B30~70) showed a linear structural degradation from the original scenes. In

contrast, the rats with DG lesion showed non-linear impairment patterns, where they were able to perform normally in less blurred conditions and impaired in only highly blurred conditions. Future studies may employ other ways of morphing two scenes that severely degrades the structural layout of the original scenes.

Chapter 2. Impaired pattern separation in scene-dependent rate modulation in CA3 single units following the lesion of the dentate gyrus

Introduction

Computational theories on the hippocampus suggest that DG-CA3 circuitry is important for pattern separation and completion, two key processes which are seemingly opposite computational processes but are essential in classifying current environment based on prior experience (O'Reilly and McClelland, 1994; Treves and Rolls, 1994; Rolls and Kesner, 2016). A handful of studies have investigated how the perturbation of the DG affected place cell activities in the CA3 (McNaughton et al., 1989; Sasaki et al., 2018; van Dijk and Fenton, 2018; Lee et al., 2019). However, these studies did not use behavioral tasks in which rats had to make explicit choices using the computational processes supported by the DG-CA3 circuit, and the exact mechanism in which such processes occur on a single-unit level remains unclear.

In this part of the thesis, I will present electrophysiological evidence on the effect of DG lesion on the pattern separation of scene-dependent firing activities in the CA3 single units, when the rats were required to make choices based on degraded scene inputs.

Materials and methods

Electrophysiological recording

After a five-day recovery period, rats were retrained (~160 trials per session using the same pairs of scenes used before surgery) until they showed stable performance (>75% correct choices for each scene), during which tetrodes were gradually lowered into target areas. To adjust the tetrodes, the rats were placed on a pedestal in a custom-made aluminum booth outside the behavioral testing room. Neural signals were transmitted through the headstage (HS-36, Neuralynx) and the tether attached to the electrode interface board (Neuralynx) of the hyperdrive to the data-acquisition system. Neural signals were digitized at 32 kHz (filtered at 600–6000 Hz) and amplified 1000–10,000 times. Tetrodes were lowered daily by small increments to reach the target areas.

During the behavioral task, neural signals were relayed through a slip-ring commutator (Neuralynx) to the data-acquisition system, and an array of green and red LEDs was attached to the headstage to monitor the animal's position and head direction using a digital camera on the ceiling (sampling rate at 30 Hz).

Unit isolation

Single units from the dorsal CA3 were isolated manually using custom-written software (WinClust). Various waveform parameters,

such as peak and energy, were used during the procedure as described (Delcasso et al., 2014). Neurons were included in analyses if they showed ≥ 50 spikes during an outbound journey from the start box to the food well, if the mean firing rate of the session was < 10 Hz, and if the spatial information score was > 0.2 (Table 1).

Session	Group	Complex-spiking units	Units with intact place field
Familiar	Control	58	35
	DG lesion	84	45
Blurred	Control	47	24
	DG lesion	43	16
Masked	Control	84	51
	DG lesion	61	29
Overlay	Control	71	32
	DG lesion	76	27

Table 1. The number of CA3 units included in the analysis after unit inclusion and place field definition. The number of CA3 units from each session per group are shown. Complex-spiking units were used for comparing basic firing properties and the units with intact place fields were used for rate modulation analysis.

Data analysis

Description of basic firing properties

The amount of spatial information conveyed by a unit was measured by constructing a linearized firing-rate map (Fig. 8). For this purpose, position data from a behavioral session were scaled down to a bin size of 4 cm2, and a raw spatial rate map was constructed by dividing the number of spikes by the duration of a visit for each bin. Spatial information was computed using the equation (Skaggs et al., 1993):

$$\text{Spatial information} = \sum_i p_i \frac{\lambda_i}{\lambda} log_2 \frac{\lambda_i}{\lambda} \text{ (bit/spike)}$$

, where *i* denotes the bin, p_i is the occupancy rate of the *i*th bin, λi is the mean firing rate of the ith bin, and λ is the overall mean firing rate. The mean firing rate of a unit was calculated by averaging the firing rates in the raw rate map. A burst index was defined as the power of autocorrelation during the 1–6 ms period normalized by the power during the 1–20 ms period.

Definition of the boundaries of a place field and its center

A place field was defined as three or more contiguous bins with firing rates >20% of the peak firing rate of the unit. Only CA3 units with both the start and end bins identified in a linearized firing rate map were included in the analysis for place fields (Fig. 8). The mean firing rate used to calculate the rate-modulation index were measured only within the boundaries of the unit's place field.

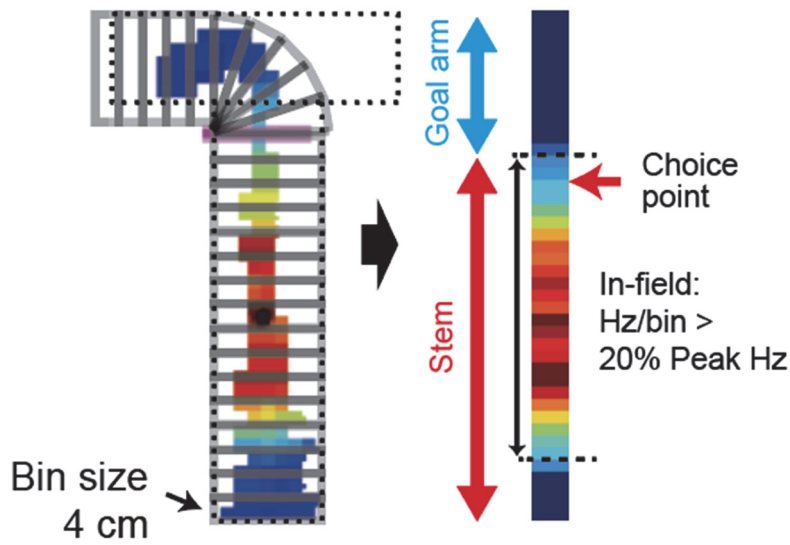

Figure 8. Illustration of the linearization process of a CA3 place field. The choice point was defined as the bin in which the trajectories for the left and right trials differed significantly for at least two consecutive bins.

Rate modulation analysis

To quantify the changes in discharge patterns of single units across different scene stimuli, a rate modulation index (RMI) was calculated using the mean firing rate of the place field for each condition. To directly compare the degrees of rate modulation during different sessions, the difference in firing rate between the left and right response-associated scene conditions was calculated as:

$$\text{RMI} = \left|\frac{mean(FR_1) - mean(FR_2)}{mean(FR_1) + mean(FR_2)}\right|$$

, where FR_1 and FR_2 denote in-field firing rates of the trials associated with the two conditions.

The rate modulation patterns across different levels of visual alterations for the scenes in the *Blurred*, *Masked,* and *Overlay* sessions were evaluated by quantifying the relationships between the mean firing rates and the levels of manipulations associated with visual scene stimuli, with these relationships visualized using a tuning curve. Due to a smaller number of correct trials observed in scene stimuli with higher difficulty levels, the mean firing rates for the last two difficulty levels in the *Blurred* and *Masked* sessions were combined (L50 and L70 into L57, R50 and R70 into R57 in the *Blurred* session; L3 and L4 into L34, R3, and R4 into R34 in the *Masked* session). The mean firing rates for eight conditions (two scenes x four ambiguity levels) were normalized from 0 to 1, using the following equation:

$$\text{Normalized FR}cond = \frac{FRcond - min(FR_{1-8})}{max(FR_{1-8}) - min(FR_{1-8})},$$

, where Normalized FR_{cond} is normalized firing rate for a condition (cond), FR_{cond} denotes mean firing rate for a condition, $min(FR_{1\text{-}8})$ and $max(FR_{1\text{-}8})$ denote the minimum and maximum value among the eight mean firing rates from each condition. Normalized firing rates were oriented so that the scene category associated with the higher firing rates were always on the right-hand side of the graph.

The tuning curve was produced by fitting the data with the following set of model equations:

(1) Quadratic model: $\alpha + \beta * (scene) + \gamma * (scene)^2$

(2) Four-parameter sigmoidal model:

$$F(x) = L + \frac{(U - L)}{1 + (scene/\alpha)^{\beta}}$$

, where L and U are the lower and upper asymptotes, respectively, the $scene$ denotes the level of manipulation for the scene stimulus, and α and β are the inflection point and slope at that point, respectively, of the sigmoidal curve (Fig. 9). The quadratic model and sigmoidal model were compared using the Bayesian information criterion (BIC), where the model with the lower BIC value was defined as the best one to explain the unit data (Schwarz, 1978). The model with a better fit was displayed in a solid line along with its coefficient of determination. The two models were compared with each other to identify the single units that exhibited a categorical response near the optimal decision point (defined by the task demand). Specifically, if a unit showed a categorical response across different

levels of ambiguity, the neural activities should be better explained by the sigmoidal model than by the quadratic model (Fig. 9). However, if a unit exhibited gradual changes, it should be fit better by the quadratic model than by the sigmoidal model (Fig. 9). The proportions of units better explained by the sigmoidal model were compared in the control and DG-lesion groups using Chi-square tests for within-session comparisons and Z-score tests for comparing across different sessions. This analytical strategy was previously used to successfully differentiate functional classes of cells in the perirhinal cortex during an object recognition task (Ahn and Lee, 2017).

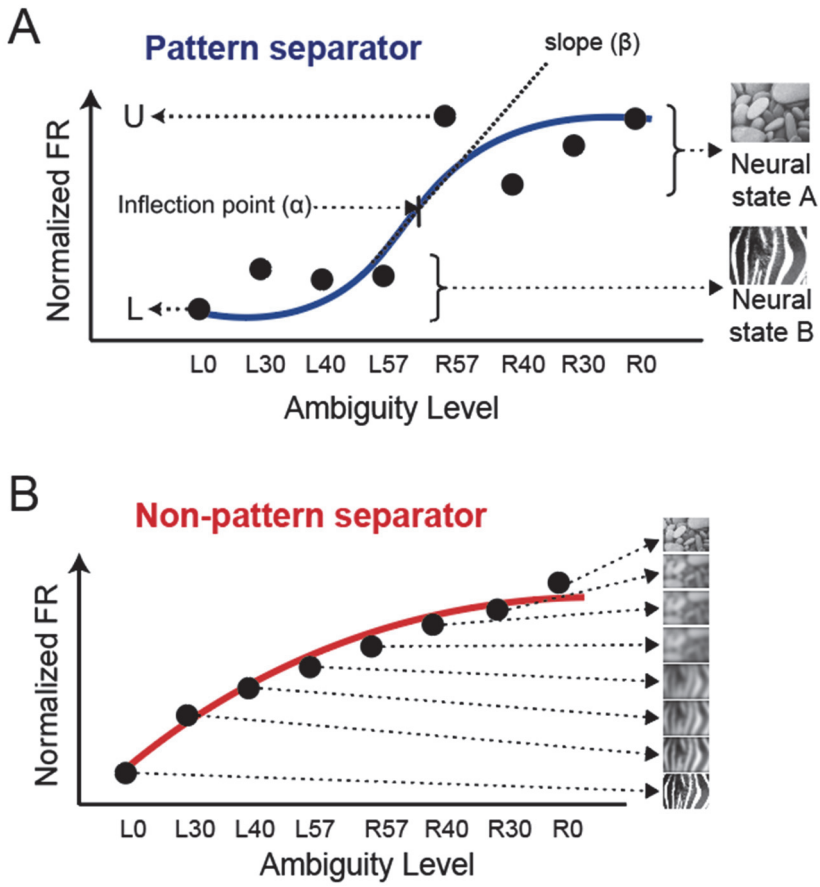

Figure 9. Sigmoidal and quadratic model estimation for scene-tuning curves in the CA3 units. (A) Illustration of the four-parameter sigmoidal model used to evaluate the stepwise and categorical rate modulation across ambiguous visual scenes. The 'neural state' denotes the median normalized firing rate (FR) of the points above and below the inflection point. U: Upper asymptote, L: Lower asymptote. (B) Illustration of the quadratic model used to evaluate the gradual rate modulation across ambiguous visual scenes.

The linear model and three-parameter sigmoidal model, which are reduced forms of the quadratic model and the sigmoidal model, were also used for the scene-tuning curve estimation. The linear model is identical to the quadratic model, except that the third term (γ) was removed. For the three-parameter sigmoidal model, the upper and lower asymptotes were combined as a single parameter.

To assess the tuning curve on a population level, each unit's normalized mean firing rates were reoriented based on the sign of the slope of the better-fitted model in the individual model fitting results. Reoriented normalized mean firing rates were averaged for each of eight levels, separately for the control and lesion groups, to produce the population mean firing rate for each scene category. Estimation of the scene-tuning curve for the population data was performed in the same manner as for individual units as described above.

Local field potential (LFP) analysis

The LFP data from tetrodes that were located in the CA3 cell layer and showed more than five well-isolated clusters were down-sampled from 32 kHz to 2 kHz using the CSC File Rate Reducer program (Neuralynx). Down-sampled LFP data were analyzed with a custom-written script implemented in MATLAB (Mathworks). The LFP data were separated into two data sets by applying two different frequency ranges. First, the LFP data for ripple frequency range (150 Hz – 250 Hz) were bandpass-filtered with following parameters:

Passband edge frequency (Wp): 145 Hz – 255 Hz

Stopband edge frequency (Rp): 130 Hz – 270 Hz

Passband ripples (Rp): 3 dB

Stopband attenuation (Rs): 15dB

To identify movement-related artifacts, the LFP data were filtered using a different frequency, ranging from 350 Hz to 450 Hz. The following parameters were applied for noise detection:

Passband edge frequency (Wp): 345 Hz – 455 Hz

Stopband edge frequency (Rp): 330 Hz – 470 Hz

Passband ripples (Rp): 3 dB

Stopband attenuation (Rs): 15dB

Both ripple frequency and noise frequency filtered LFP data were then smoothed by a Gaussian filter (bin size: 25/2000 s).

Sharp-wave ripple (SWR) detection

To identify SWR events during the recording sessions, filtered LFP data were applied with the Hilbert transform and smoothed with a Gaussian filter (bin size: 25/2000 s). The envelope from the ripple-frequency data (150 Hz – 250 Hz) was defined as the period where the signal exceeded 2 times of standard deviation (S.D.) from the mean. Ripple events whose durations were less than 20 ms were discarded and events with intervals with less than 20 ms were considered as one event.

To identify the movement-related artifacts, the velocity of the animal during the behavior session, and the noise-frequency envelopes during the entire session (pre-sleep/behavior/post-sleep sessions)

were analyzed. Ripple events were considered void, 1) if the velocity of the rat exceeded 5 cm/s in more than half of the ripple duration, 2) or if ripple event did not co-occur at least two tetrodes, 3) or if the ripple co-occurred with a noise event. A noise event was defined in an identical method to ripple event, except that the procedure was applied to the noise frequency data.

Experimental design and statistical analysis

Differences in unit firing properties were compared by Kolmogorov–Smirnov tests (K-S test), with the level of statistical significance set at $\alpha = 0.05$, implemented in StatView software package (SAS Institute, Cary, NC). Chi-square tests for independence, implemented in JMP11, was used for comparing the proportions between the groups within a session. Z-score tests were used for comparing two proportions associated with different sessions. A two-way ANOVA (group, session type as factors) were run in JMP 11 to compare the difference in the coefficient of determinations (R^2) from the sigmoidal model fit. The results of post-hoc t-tests for ANOVA comparing session type and group were corrected using a Bonferroni correction procedure for multiple comparisons.

Results

Tetrode locations along the transverse axis were unaffected by DG lesions

To assess whether there were any differences in tetrode tracks between two groups, we identified AP and ML coordinates of all the tetrodes in which any unit was recorded during the entire sessions (Fig. 2C). There was no significant difference between two groups in both AP and ML coordinate distributions (AP: $\chi^2_{(2)} = 6.624$, $p = 0.073$, ML: $\chi^2_{(2)} = 1.989$, $p = 0.74$, KS test). Similarly, there was no significant difference between the two groups in the relative recording locations ($\chi^2_{(2)} = 4.764$, $p = 0.185$, Fig. 2D). This result indicates that the differences found between two groups unlikely to be caused by the functional heterogeneity along the proximodistal axis of the CA3 (Lee et al., 2015).

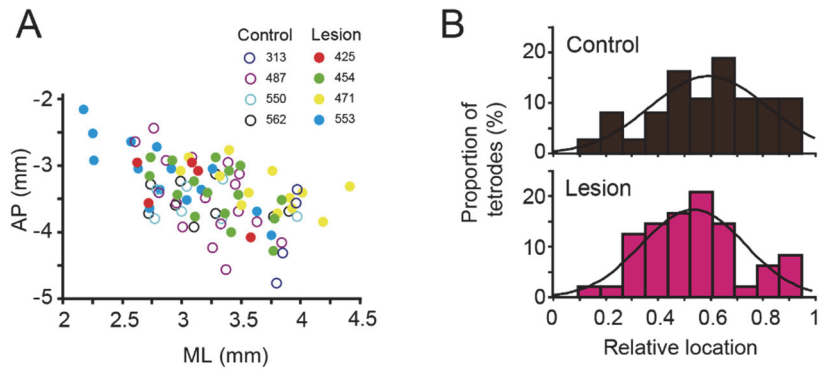

Figure 10. Verification of recording locations within the CA3. (A) Distribution of the AP and ML coordinates of tetrodes. Tetrodes from control rats are depicted as open circles and those of the DG-lesioned rats are as filled circles. Individual rats are shown in different colors. (B) Distribution of the relative locations of the tetrodes in the control and DG-lesion groups. The relative location of 1 denotes the boundary between CA3 and CA2. The black curves denote estimated normal distribution.

Basic firing properties were unaffected by DG lesions

Despite the absence of DG inputs, there was no significant difference in raw spike waveforms (Fig. 11A, B). Spike width ($\chi^2_{(2)}$ = 5.45= , p = 0.131, KS test), burst index ($\chi^2_{(2)}$ = 4.29, p = 0.233, KS test), mean firing rate ($\chi^2_{(2)}$ = 3.84, p = 0.293, KS test) and peak firing rates ($\chi^2_{(2)}$ = 6.61, p = 0.073, KS test) in CA3 units recorded during the Familiar sessions did not differ significantly between the lesion and control groups (Fig. 11C, D). Intact place cells were observed in the CA3 during the VSM task in both control group (Fig. 12A) and DG-lesion group (Fig. 12B), which is consistent with the previous studies reporting intact spatial selectivity of CA3 cells after the DG lesion (McNaughton et al., 1989).

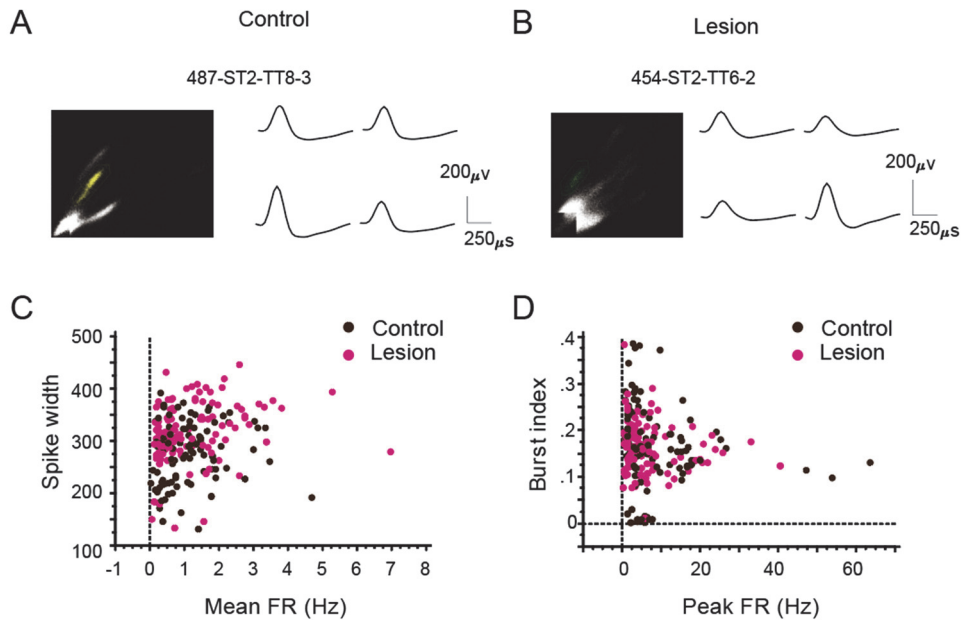

Figure 11. Basic firing properties of CA3 neurons during Familiar sessions. (A) Raw spike waveform examples from control group. The average spike waveforms from four channels of a tetrode are shown. The scale bars indicate waveform amplitude (vertical) and width (horizontal). (B) Raw spike waveform examples from DG lesion group. (C) Scatterplot for spike width and mean firing rate, peak firing rate, burst index) of CA3 cells from the two groups during the Familiar sessions (N = 142 neurons). No significant differences were observed. . (D) Scatterplot for burst index and peak firing rate of CA3 cells from the two groups during the Familiar sessions. No significant differences were observed.

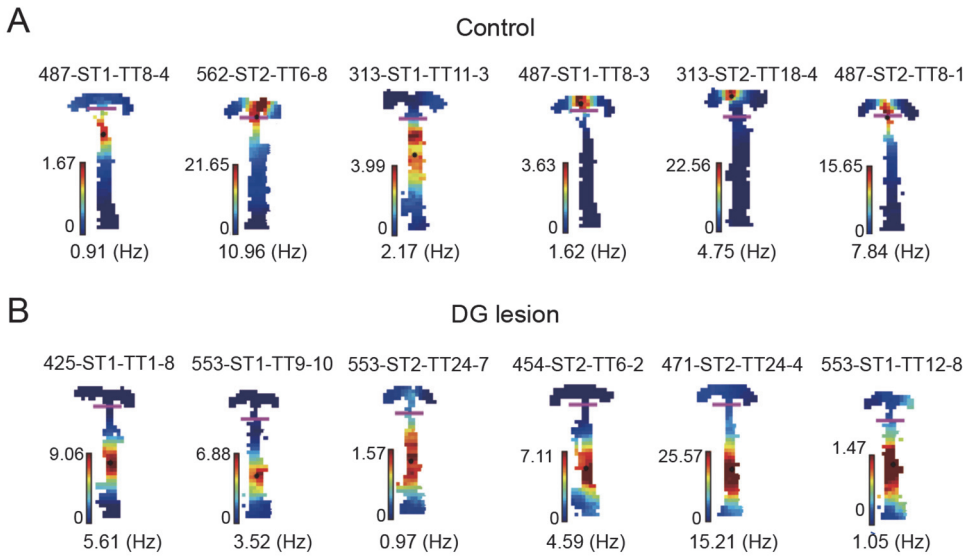

Figure 12. Individual examples of CA3 place cells in the *Familiar* sessions. (A) Examples of spatial firing patterns of CA3 units with intact DG. Cell identities are marked on top of the unit examples, which denote information about the rat, session, tetrode and cluster identity of each unit in that order. Numbers on the top of the color bar indicate a peak firing rate. In-field mean firing rates are shown below each spatial firing rate map. Black dots indicate the center of mass of the place field. (B) Examples of spatial firing patterns of CA3 units from rats with DG lesions.

Categorical rate modulation in the CA3 across ambiguous scenes occurs in the control, but not the DG-lesion, group

Pattern separation is a computational process that reduces the amount of overlap in output patterns using similar input patterns (O'Reilly and McClelland, 1994; Treves and Rolls, 1994). To test if pattern separation occurred in the CA3 for ambiguous visual scenes in the VSM task, the neuronal firing rates for ambiguous scenes, including the originals, were calculated from the place fields defined on a linearized rate map (Fig. 8). For each unit, the firing rates across different scene stimuli were normalized and the difference (rate-modulation index [RMI_{LR}]) between the firing rates for the left and right choice-associated scenes was determined. Although the degree of rate modulation between left and right scenes was similar in the Familiar session for both groups ($Z = -0.05$, $p = 0.960$, Mann-Whitney U test, Fig. 13), rate modulation was lower in the DG-lesion group when ambiguity was introduced into the scene stimuli during the *Blurred* sessions ($Z = -2.04$, $p = 0.041$, Mann-Whitney U test). However, the group differences in rate modulations were not observed during the *Masked* ($Z=1.02$, $p = 0.307$, Mann-Whitney U test) or *Overlay* sessions ($Z = -0.411$, $p = 0.681$, Mann-Whitney U test).

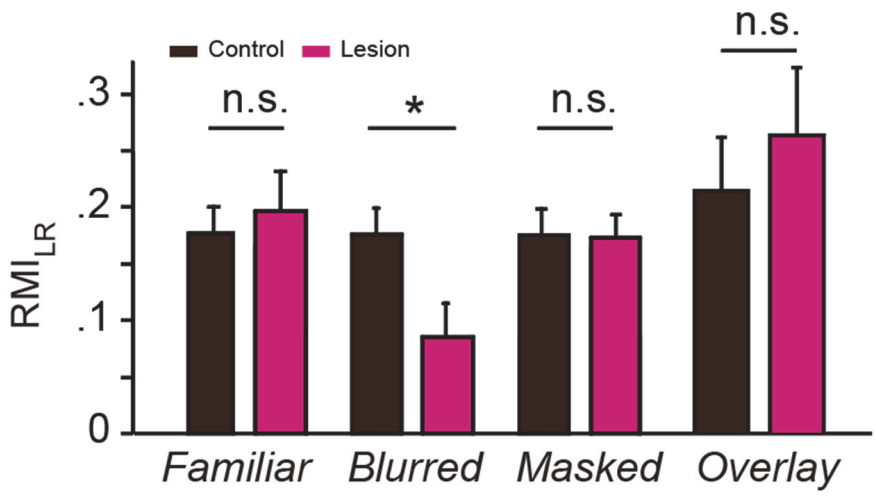

Figure 13 Scene-dependent firing rate modulation in the CA3 during the VSM task. Rate modulation index (RMI) between the left and right response-associated scenes in the *Familiar, Blurred, Masked and Overlay* sessions are shown. Mean ± standard error. n.s.: not significant, *$p < 0.05$.

Firing-rate tuning curves for visual scenes were subsequently determined for individual CA3 cells. Place cells in the CA3 showing a categorical tuning curve across the blurred scene stimuli according to their choice contingency were regarded as pattern separators (Fig. 9A). In contrast, place cells in the CA3 showing a gradual change in firing rates across the blurred scenes were regarded as non-pattern separators (Fig. 9B). To objectively determine the categorical nature of neuronal firing for the scene stimuli, the normalized firing rates of a cell were fitted using two models, i.e., a sigmoidal model that for fitting stepwise (or categorical) data (Fig. 9A) and a quadratic model for fitting gradually changing data (Fig. 9B). The model that better fits the data was regarded as the tuning curve of the cell.

To test the validity of the unit-categorizing procedures described above, we first fit all units (N= 179 neurons) from three session types (*Blurred*, *Masked* and *Overlay*) using the sigmoidal model (including the ones from the units better fit by the quadratic models) to quantify the similarity between the two scene representations coded by the neural states (measured by median) above and below the inflection point (Fig. 9A). The distance between the neural states was larger in the pattern separators than in the non-pattern separators, meaning that the pattern separating neurons coded ambiguous stimuli into more discrete states ($\chi^2_{(2)}$ = 32.754, p = 0.001, K-S test) (Fig. 14A). The unit-categorization procedure seemed valid because, the units whose tuning curves for scenes were fit better by sigmoidal models (i.e., pattern separators) showed tighter fitting than those fit by

quadratic models (i.e., non-pattern separators) ($\chi^2_{(2)}$ = 53.175, p = 0.001, K-S test) and had inflection points located closer to the midpoint of the ambiguity levels ($\chi^2_{(2)}$ = 27.281, p = 0.001, K-S test) (Fig. 14B).

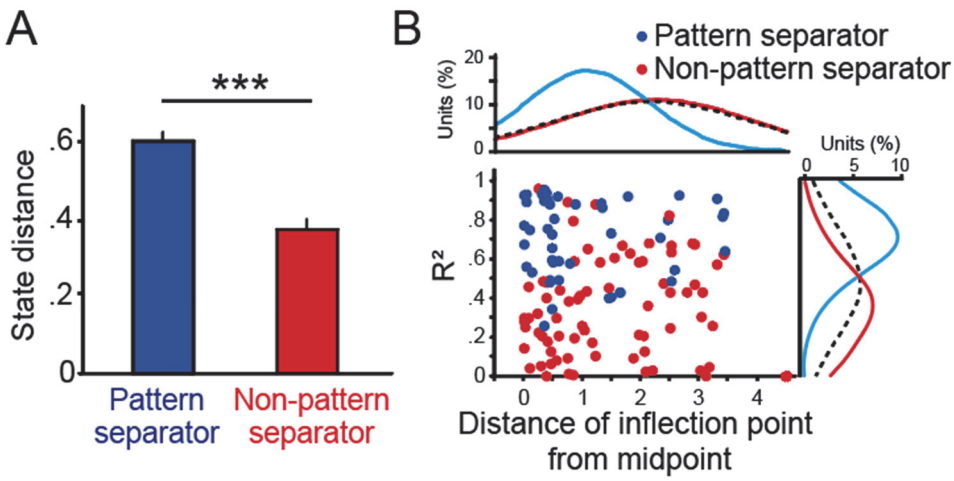

Figure 14. Characterization of two different unit types using model comparison analysis. (A) State distance (i.e., the distance between neural state 1 and 2 in Fig. 5A) between two categorical responses of the pattern separator and non-pattern separator cells from the *Blurred*, *Masked* and *Overlay* sessions. Mean ± standard error. ***p < 0.001. (D) Scatterplot showing the correlation between the coefficient of determination (R^2) and the distance of the inflection point from the midpoint of ambiguity levels from the *Blurred*, *Masked* and *Overlay* sessions (N = 179 neurons). The unit types defined by the BIC comparisons are depicted in different colors. The percent unit distribution on the right-hand side shows the R^2 distributions for the pattern separators (blue), non-pattern separators (red), and all cells together without any functional categorization (black dotted line). The percent unit distribution on the top shows the distance distributions for the pattern separators (blue), non-pattern separators (red), and all cells together without any functional categorization (black dotted line).

We found that the scene-related firing patterns of the CA3 cells in the control group were better to fit by the sigmoidal model than the quadratic model (Fig. 15A), and vice versa for the lesion group (Fig. 15B). That is, pattern separators were more frequently found in the control group than in the lesion group and vice versa for non-pattern separators.

The goodness of fit for the sigmoidal model (measured by the coefficient of determination) was significantly higher on average in the control group (N = 24) than in the lesion group (N = 16) during Blurred sessions ($\chi^2_{(2)}$ = 9.60, p = 0.016, K-S test) (Fig. 16A). The inflection points were also distributed closer to the optimal decision point in the control group than in the lesion group ($\chi^2_{(2)}$ = 8.817, p < 0.05, K-S test) (Fig. 16A). The proportion of pattern separator-like cells was significantly lower in the DG-lesion than in the control group in the Blurred session ($\chi^2_{(1)}$ = 5.934, p = 0.015, Chi-square test) (Fig. 16B). The attenuation of pattern separator-like activity was also observed at a population level. That is, the population tuning curve for visual scene in the DG-lesion group was similarly explained by the sigmoidal model (BIC = -15.12) and quadratic model (BIC = -14.59), whereas the sigmoidal model explained the neural firing more powerfully in the control group (BIC = -26.62 for sigmoidal model; BIC = -23.29 for quadratic model) (Fig. 16C and 16D). These findings suggest that the behavioral impairment observed in rats with DG lesions (Fig. 4 and 5A) may be related to the degradation of discrete memory representations for similar visual scenes.

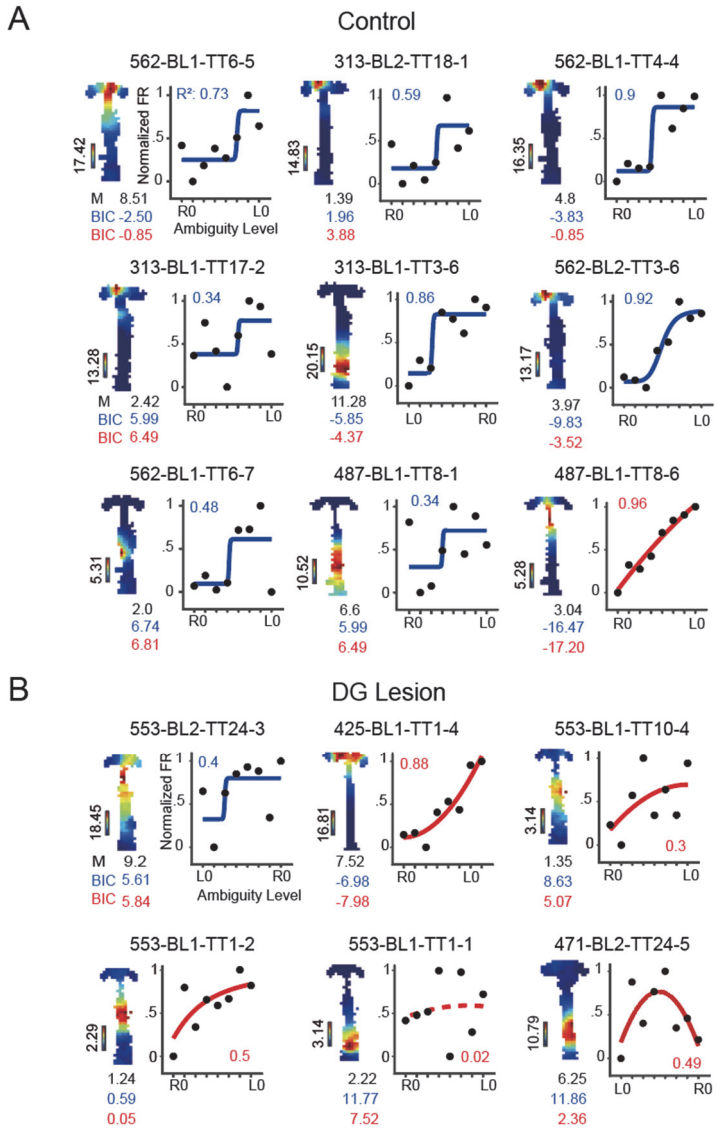

Figure 15. Individual examples of CA3 place cells in the *Blurred* sessions. (A) Examples of stepwise rate modulation in the CA3 units with intact DG. M denotes the in-field mean firing rate, R^2 denotes the goodness of fit of the better explaining model. BIC values (blue from the sigmoidal model and red from the quadratic model) used for the categorization are shown below the rate map. Blue lines indicate well-fit sigmoidal models and red lines indicate well-fit quadratic models. The dotted lines indicate poor fit ($R^2 < 0.3$) of the models. (B) Examples of gradual rate modulation in the CA3 units with DG lesions.

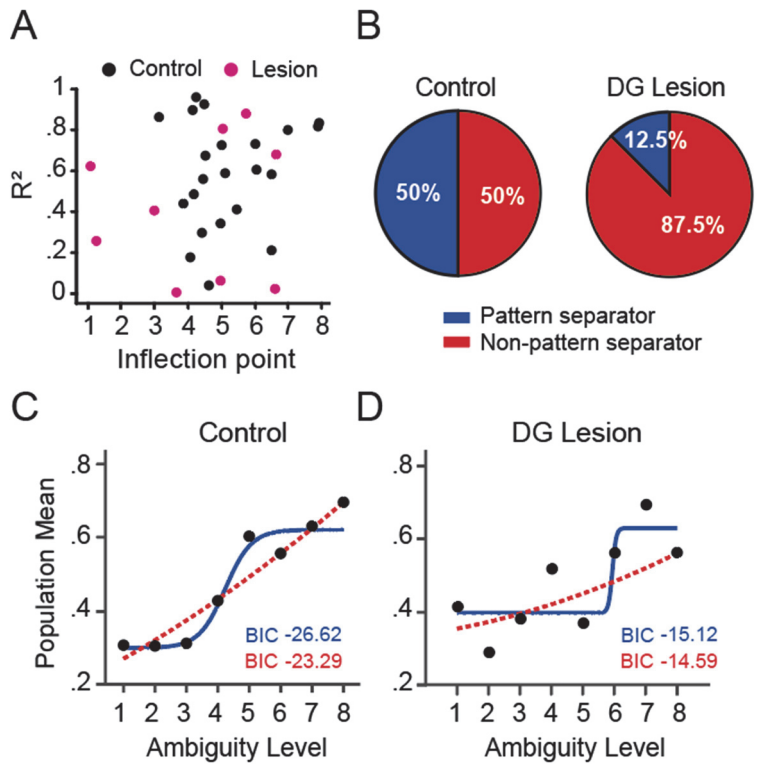

Figure 16. Disrupted categorical rate modulation in the CA3 with DG lesions. (A) Scatterplot of the inflection points and the goodness-of-fit parameters from sigmoidal model during *Blurred* sessions (N = 40 neurons). The control and lesion groups are marked in different colors. Units with inflection points lower than 1 were excluded from the plot (7 from lesion group and 2 from control group). (B) The proportions of units that are better explained by the sigmoidal model (pattern separator-like cells, blue) and by the quadratic model (non-pattern separators, red) in the control and lesion groups. (C) The population scene-tuning curve from control (left) and (D) DG-lesion group (right) in the *Blurred* sessions. BIC values from the sigmoidal model (blue) and quadratic model (red) are shown below the scene tuning curve.

It is unlikely that the abovementioned differences between the groups were caused by the inherent differences in firing rates that might be better suited for either model fitting because the place cells of the two groups during the *Blurred* sessions (N = 40 neurons) were similar to each other with respect to the in-field mean firing rate ($\chi^2_{(2)}$ = 3.267, p = 0.39, K-S test), normalized firing rate ($\chi^2_{(2)}$ = 6.667, p = 0.071, K-S test), and the standard deviation of the normalized firing rate ($\chi^2_{(2)}$ = 3.28, p = 0.39, K-S test) (Fig. 17A). To equate the parameters between the models, we also tried a reduced sigmoidal model and a linear model to estimate the scene-tuning curve. The reduced sigmoidal model was intended to match the number of parameters to that of the quadratic model. However, consolidating the upper and lower asymptotes to one parameter resulted in non-optimal fitting results in multiple units (Fig. 17B). For example, when estimating the scene-tuning curve of a unit, the reduced model showed the inflection point near the first level, followed by a steep negative slope which deviated from the scene stimuli-associated firing rates (Fig. 17C).

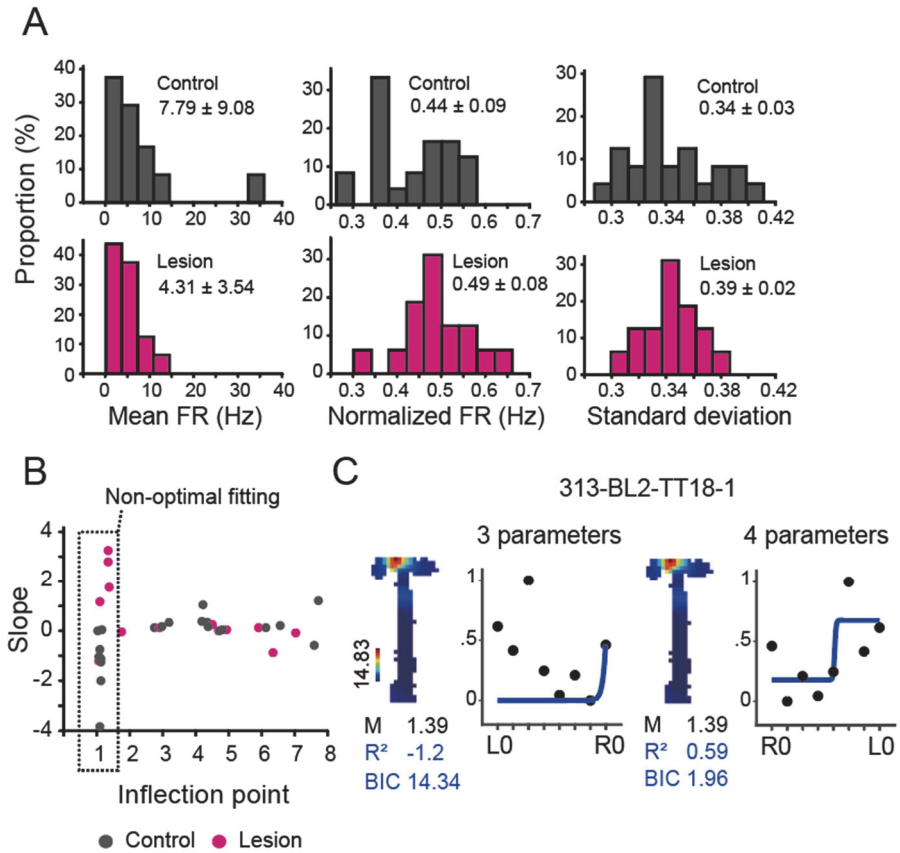

Figure 17. Alternative models for the categorical rate modulation in the CA3. (A) Distribution of the mean firing rates, normalized mean firing rates, and the standard deviation of the normalized firing rates of place cells from *Blurred* sessions (N = 40 neurons). (B) Scatterplot of the inflection points and the slope at those points, estimated by the reduced sigmoidal model using only a single parameter for both upper and lower asymptotes. The dotted box indicates the units with the non-optimal fit. (C) Example of non-optimal fit caused by the reduced model (left), shown along with the model fit result from the full sigmoidal model.

Categorical firing patterns in the CA3 for visually masked or mixed scene stimuli are not affected by DG lesions

To determine whether changes in the visual scene could cause the degradation of rate modulation in the CA3 after DG lesions, data from the *Masked* sessions, in which visual scenes were partially occluded, but the pattern itself remained visible, were analyzed. The performance of the two groups did not differ significantly during the *Masked* sessions (Fig. 5B and C), suggesting that partial occlusion of the visual scene does not affect pattern separation in the CA3 as much as does blurring of the scene.

Consistent with these behavioral results, the pattern separator-like cells were equally abundant in the DG-lesion (Fig.18B) and control (Fig. 18A) groups during the *Masked* sessions ($\chi^2_{(1)} = 0.004$, $p = 0.949$, Chi-square test). Similarly, the percentages of pattern separator-like (44.8%) and non-pattern separator-like (55.2%) cells were similar in the DG-lesion group ($Z = -0.79$, $p = 0.429$, Z-score test, Fig. 19A). The proportion of pattern separator-like cells in the CA3 of the DG-lesion group during *Masked* sessions (44.8%) was similar to that of the control group (50.9%) in the *Masked* ($Z = -0.53$, $p = 0.596$, Z-score test) and *Blurred* ($Z = -0.37$, $p = 0.703$, Z-score test) sessions, but was significantly higher than that of the DG lesion group during *Blurred* sessions ($Z = 1.75$, $p = 0.04$, Z-score test). The population tuning curves for visual scenes were similar between the two groups in the *Masked* sessions (Fig. 19B). The sigmoidal model explained the neural firing more powerfully in the

control group (BIC = -27.81 for sigmoidal model; BIC = -21.65 for quadratic model), as well as in the DG lesion group (BIC = -25.38 for sigmoidal model; BIC = -22.35 for quadratic model).

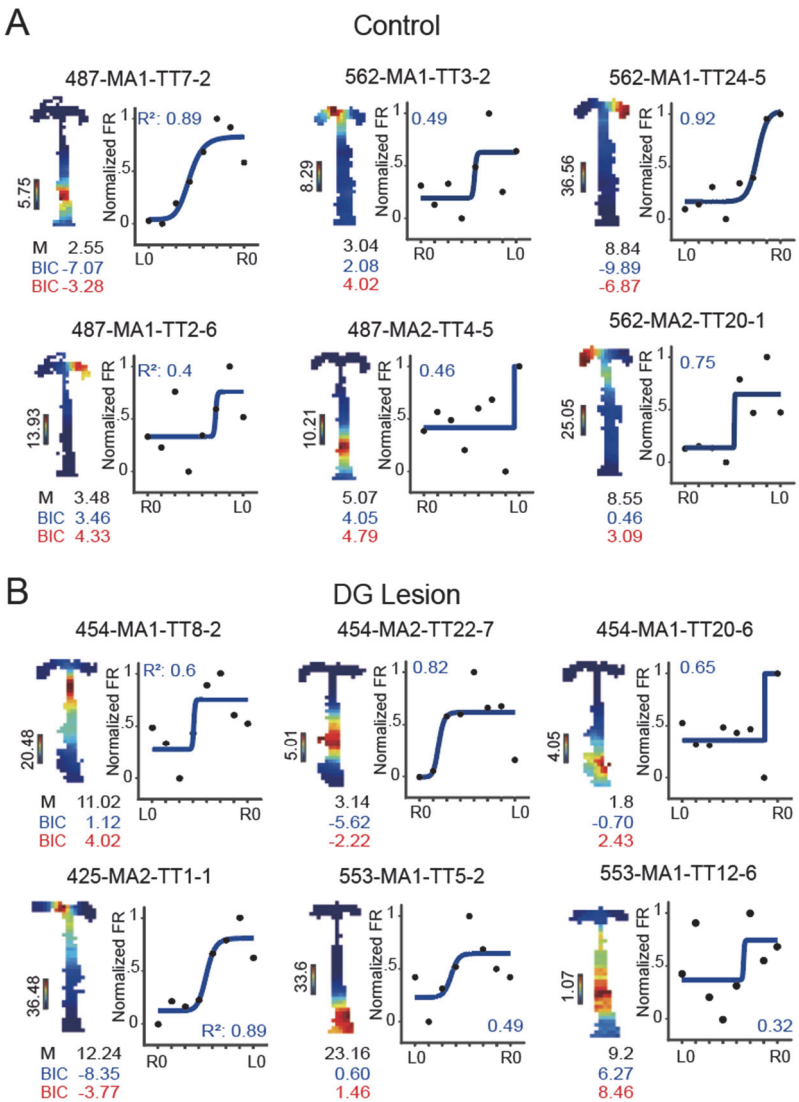

Figure 18. Individual examples of CA3 place cells during retrieval of partially occluded visual scenes. (A) Examples of stepwise rate modulation in CA3 units with intact DG, as shown in Fig. 6A. Blue lines indicate well-fit sigmodal models. BIC values (blue from the sigmoidal model and red from the quadratic model) used for the categorization are shown below the rate map. (B) Examples of categorical rate modulation in CA3 units with DG lesions.

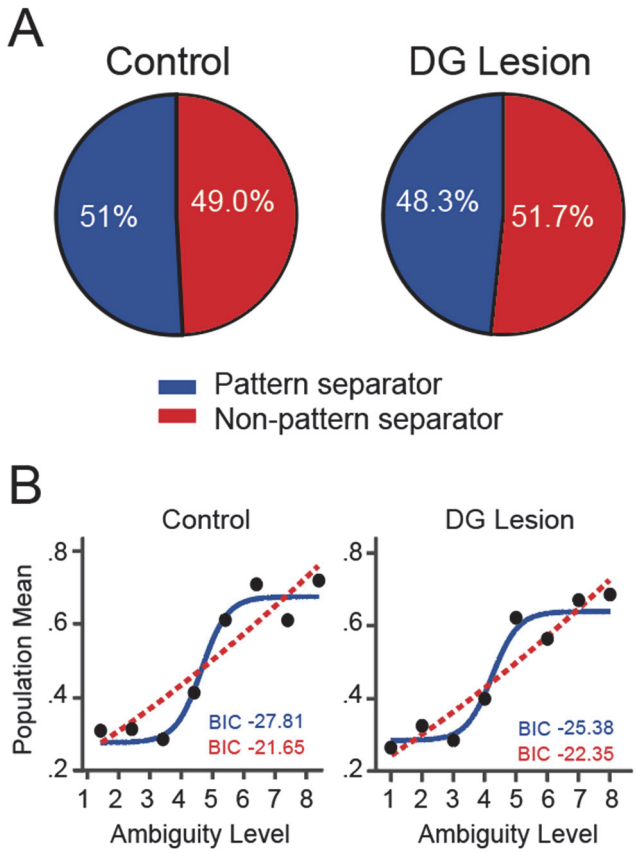

Figure 19. Scene-dependent rate modulation in the CA3 during retrieval of partially occluded visual scenes. (A) The proportion of units that were better explained by the sigmoidal model (pattern separator-like cells, blue) and by the quadratic model (non-pattern separator-like units, red) in the control and DG lesion groups during the *Masked* sessions. (B) The population scene-tuning curve from control (left) and DG-lesion group (right) in the *Masked* sessions. BIC values from the sigmoidal model (blue) and quadratic model (red) are shown below the scene tuning curve.

Similar to the *Masked* session, performance in the *Overlay* session was not affected by DG lesions. During the *Overlay* session, pattern separator-like cells were as frequently found in the DG-lesion group (Fig. 20B and 21A) as in the control group (Fig. 20A) ($\chi^2_{(1)}$ = 0.003, p = 0.957, Chi-square test). Similarly, the population tuning curves for visual scenes were similar between the two groups in the *Overlay* sessions (Fig. 21B). The sigmoidal model explained the neural firing more powerfully in the control group (BIC = -28.82 for sigmoidal model; BIC = -14.23 for quadratic model), as well as in the DG lesion group (BIC = -21.57 for sigmoidal model; BIC = -16.09 for quadratic model).

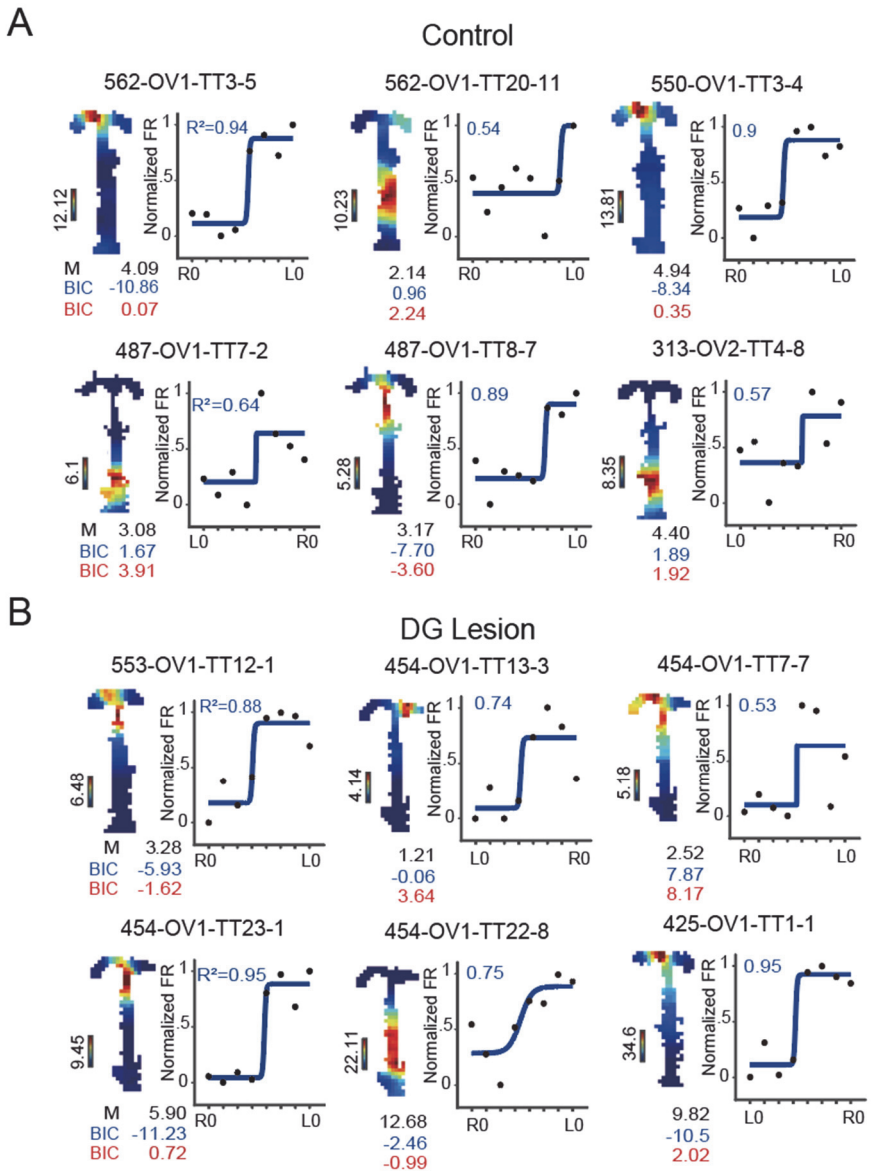

Figure 20. Individual examples of CA3 place cells in the *Overlay* sessions. (A) Examples of stepwise rate modulation in CA3 units with intact DG, as shown in Fig. 6A. Blue lines indicate well-fit sigmodal models. BIC values (blue from the sigmoidal model and red from the quadratic model) used for the categorization are shown below the rate maps. (B) Examples of categorical rate modulation in CA3 units with DG lesions.

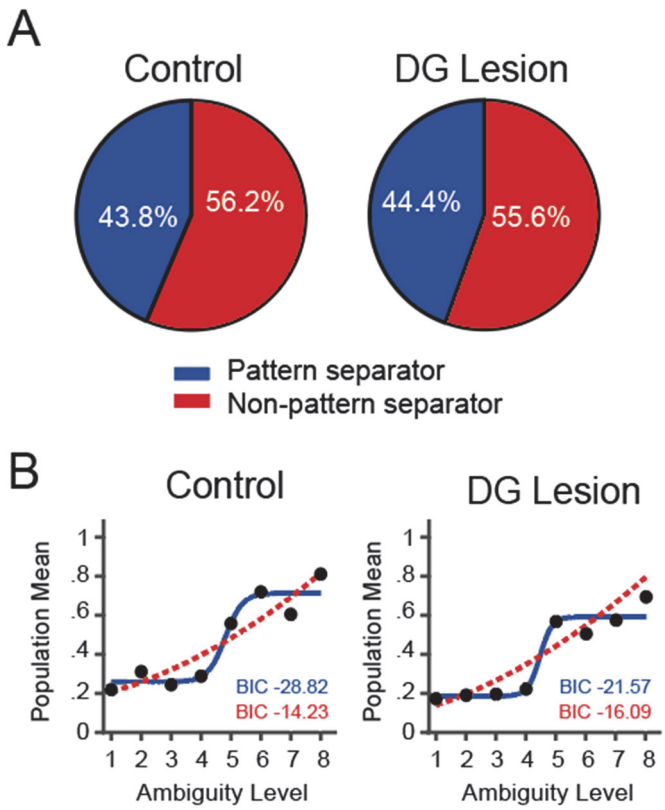

Figure 21. Scene-dependent rate modulation in the CA3 during the retrieval of partially mixed visual scenes. (A) The proportion of units that were better explained by the sigmoidal model (pattern separator-like cells, blue) and by the quadratic model (non-pattern separator-like units, red) in the control and DG lesion groups during the *Overlay* sessions. (B) The population scene-tuning curve from control (left) and DG-lesion group (right) in the *Overlay* sessions. BIC values from the sigmoidal model (blue) and quadratic model (red) are shown below the scene tuning curve.

Comparing the goodness-of-fit of the sigmoidal model across three session types revealed a significant interaction between the group and session type factors ($F_{(2,173)} = 3.904$, $p = 0.022$, two-way ANOVA) only during the *Blurred* session ($t_{(173)} = -3.401$, $p = 0.001$, Bonferroni-corrected), but not in the *Masked* ($t_{(173)} = -1.241$, $p = 0.216$, Bonferroni-corrected) or *Overlay* session ($t_{(173)} = 0.20$, $p = 0.842$, Bonferroni-corrected) (Fig. 22).

These findings indicate that impaired performance of DG-lesioned rats during *Blurred* sessions was not due to any visual changes in original, familiar scenes. Altering the original visual scenes in such a way that rats could still see the overall patterns in the stimuli did not significantly disrupt performance as much as using blurred scenes. Moreover, the relatively robust stepwise tuning curves of the CA3 cells in the DG-lesioned rats maybe the neural correlates of such robust performance in the lesion group.

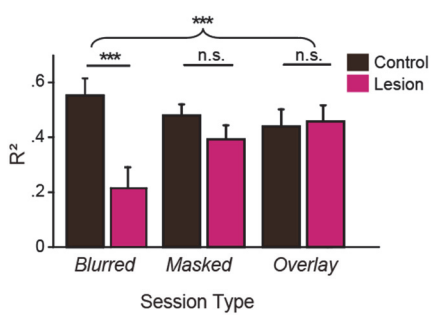

Figure 22. Degree of categorical rate modulation across altered scene conditions. The coefficient of determination (R^2) of the sigmoidal model fit from the control and DG-legion groups across the *Blurred*, *Masked,* and *Overlay* sessions are shown. Mean ± standard error. ***$p < 0.001$.

Selective DG lesions eliminate the concentration of CA3 place fields near the choice point

Normally in the VCM task, place fields tend to over-represent the choice region of the T-maze, and DG lesions seemed to eliminate such properties of place cells, a finding reported in other goal-directed tasks (Kobayashi et al., 1997; Wood et al., 2000; Lee et al., 2006). Similar results were observed in the current study. That is, CA3 place cells whose firing fields were near the crossroad of the T-maze were not uncommon in the control group (Fig. 12A). In the DG-lesion group, however, such spatial bias in field location was rarely observed (Fig. 12B). Differences in spatial bias were likely not due to any special occupancy patterns for positions, as session ($F_{(2,2)}$ = 1.09, p = 0.35), group ($F_{(1,1)}$ = 0.18, p = 0.68), and their interaction ($F_{(2,2)}$ = 1.03, p = 0.37) did not significantly affect median latency.

This phenomenon was described more quantitatively by linearizing the two-dimensional firing field (Fig. 8), followed by measuring the center of each place field relative to the center of mass (COM) in the linearized place field. When the distributions of the COM positions of all place fields in the CA3 were compared in the control and DG-lesion groups, it was clear that the place cells in the CA3 in the DG-lesion group underrepresented the choice location of the maze, defined as the first bin in which left and right trials showed significantly different lateral positions for at least two consecutive bins and differed significantly with those recorded in the control group (Fig. 23A, Z = 3.24, p < 0.01). However, the under-

representation of the choice region were not correlated rate modulation types and did not show session-specific differences (Fig.23B).

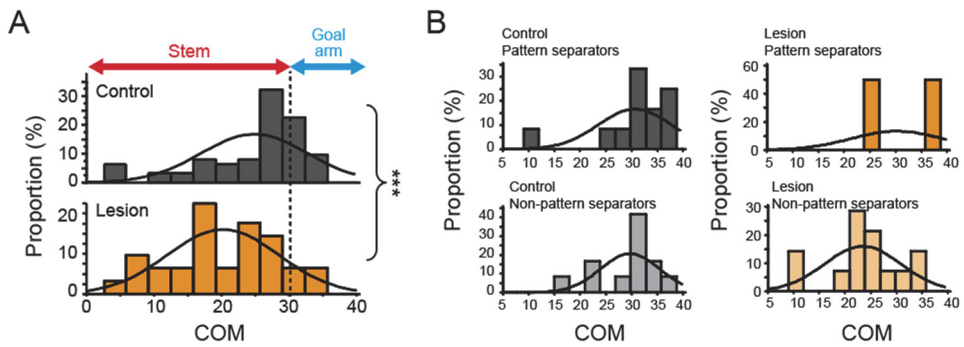

Figure 23. Spatial firing characteristics of CA3 cells with DG lesions. (A) The difference in the distribution of place-field locations (COM) in CA3 cells from the two groups from the Familiar sessions. The vertical dotted line indicates the choice point that was positioned at the border between the stem and reward locations. ***p<0.001. (B) The difference in the distribution of place-field locations (COM) in pattern separators and non-pattern separators from the *Blurred* sessions.

Selective DG lesions affected SWR patterns regardless of session type

Sharp-wave ripples (SWRs) found in the hippocampal LFP are suggested to support memory consolidation and spatial learning (Jadhav et al., 2016; Sasaki et al., 2018). Therefore, we examined the effect of DG lesions on how SWR occurrence patterns in the CA3 (Fig. 24A). In the control group, the ratio between SWR events observed during the post-sleep sessions was higher compared to the pre-sleep sessions. Interestingly, the bias toward the post-sleep sessions were attenuated by DG lesion ($F_{(1,1)} = 16.997$, $p < 0.001$). However, the attenuation of the post-sleep session bias was observed across all session types (session type: $F_{(3,3)} = 1.714$, $p = 0.165$; interaction: $F_{(3,3)} = 0.845$, $p = 0.471$).

A previous study by Leutgeb group has also reported that damages to the dentate gyrus reduced SWR events near the goal location. Therefore, we analyzed the proportion of SWR events that occurred in the arm during the behavior session (Fig. 24B). Compared to the control group, the DG lesion group had lower proportion of SWR occurrences in the arm area (group: $F_{(1,1)} = 21.567$, $p < 0.001$), regardless of session type (session type: $F_{(3,3)} = 1.416$, $p = 0.239$; interaction: $F_{(3,3)} = 1.058$, $p = 0.368$).

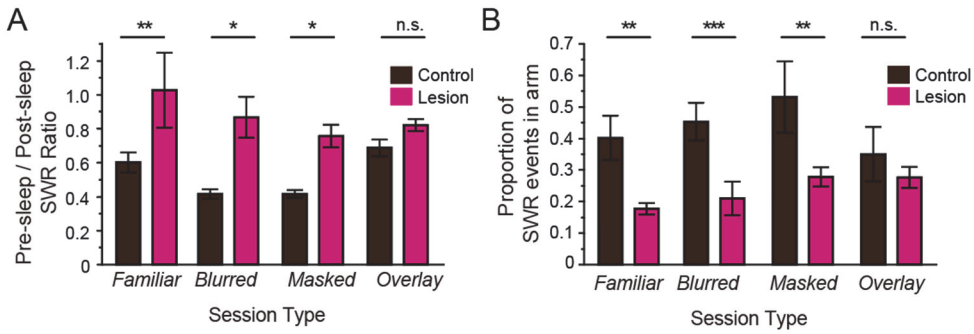

Figure 24. SWR occurrence patterns affected by DG lesions. (A) SWR ratio between SWR events in the pre-sleep session and post-sleep session across different session types are shown. n.s.: not significant, *p<0.05, **p<0.01,***p<0.001. (B) The proportion of SWR events in the arms of the T-maze during the behavior session is shown.

Discussion

This thesis is the first study to have identified the effect of the DG lesions on pattern separation processes occurring in CA3 single units during retrieval. The current study showed that rats with severe damage to the DG were impaired in processing ambiguous scenes, but not when the scenes were unaltered. Corroborating these behavioral results, scene-associated rate modulation in the CA3 was weaker in rats with DG lesions than rats with intact DG. Also, fewer pattern separator-like cells were present in the CA3 of rats with than without DG-lesions. These neural findings were specific to conditions in which the original scenes were made ambiguous by blurring, but not to conditions in which the original scenes were masked to allow rats to recognize the overall visual patterns in scene stimuli.

The degradation of the pattern separation in the CA3 units may have been driven by unstable firing rates across different scene stimuli. However, we did not find any differences in the variance of normalized firing rates between the control and DG lesion group (Fig. 17A). In addition, the goodness-of-fit for the quadratic model, which were measured in R2, did not show significant group differences in the Blurred sessions ($\chi^2_{(1)} = 4.817$, $p = 0.180$, K-S test). Therefore, it is unlikely that the impaired pattern separation in CA3 units with DG lesions was caused by unstable firing rates.

We have also reported changes in the CA3 activity that were affected by the lesion but did not depend on the type of modification

made to scenes. Cells in the DG-lacking CA3 network tended to under-represent the choice point in the maze compared with controls. In the LFP signals, rats with DG lesions showed a reduced proportion of SWR events occurring near the goal location. Reductions in DG inputs have been reported to reduce reward-related activity in the CA3 (Sasaki et al., 2018). It is difficult to provide a mechanistic explanation of this phenomenon because the underlying neural mechanisms by which place cells over-represent motivationally or strategically important areas in space during goal-directed navigation remain unclear when compared with random foraging (Eichenbaum et al., 1987; Kobayashi et al., 1997; Hollup et al., 2001; Hok et al., 2007; Dupret et al., 2010; McKenzie et al., 2013; Brown et al., 2014). Inputs from the DG may be critical for the CA3 network to reliably slow down the rats at the vantage point of the maze optimal for analyzing the visual scene and making decisions. Moreover, backpropagation of associative plasticity from the reward location may attract the place fields toward the reward locations in the hippocampus (Lee et al., 2006), with the DG playing key roles in this type of reward-based synaptic plasticity, perhaps involving dopamine, in the hippocampus (Mu et al., 2011; Gonner et al., 2017).

General Discussion

Computational, behavioral and physiological studies have shown that the DG-CA3 networks are essential in pattern separation (Marr, 1971; O'Reilly and McClelland, 1994; Treves and Rolls, 1994; Gilbert et al., 2001; Leutgeb et al., 2007; Bakker et al., 2008; Lee and Solivan, 2010; Nakashiba et al., 2012; Ahn and Lee, 2014; Neunuebel and Knierim, 2014; GoodSmith et al., 2017; van Dijk and Fenton, 2018). Behavioral evidence of pattern separation in the DG-CA3 networks was obtained predominantly using spatial memory tasks, in which rats were required to distinguish among similar spatial locations or environments (Gilbert et al., 2001; Nakashiba et al., 2012; van Dijk and Fenton, 2018). In contrast, most physiological studies have recorded cells in the DG or CA3 when rats forage for randomly scattered food, not during the performance of memory tasks (GoodSmith et al., 2017; Senzai and Buzsaki, 2017). The results of our study may fill the gap between behavioral and physiological results, by showing that CA3 cells require the DG network to physiologically display the characteristics of the pattern separating unit, including categorical and orthogonal coding of similar environmental stimuli. The absence of these pattern separator-like CA3 units in the DG-lesion group impaired their performance in *Blurred* sessions.

One of the models explaining the roles of the DG in

facilitating pattern separation emphasizes its ability to provide sparse, yet powerful inputs via mossy fibers to a small subset of CA3 cells during the acquisition of memory (Treves and Rolls, 1994). The subset of cells chosen by the sparse inputs of the DG may form a critical node, resulting in a rich Hebbian association of environmental stimuli mostly fed via the perforant path from the entorhinal cortex. This model suggests that these memory representations in the CA3 network can be retrieved mostly by the cues provided via the perforant path and that the DG may not be involved in the retrieval of memory. Although these results may seem to disagree with predictions made by these computational models, because DG lesions impaired rat performance during *Blurred* sessions, performance deficits were not observed when the original visual scenes were unaltered, partially occluded, or blurred slightly (Fig. 5).

The previous computational models simulated the retrieval mostly of the original representations from the CA3 using partial and/or noisy cues (O'Reilly and McClelland, 1994). A partial cue is defined as being a subset of the original activity patterns and a noisy cue is defined as being a combination of a subset of the original activity patterns and extra noise (O'Reilly and McClelland, 1994). When partial cues are given, the pattern completion process alone is suggested to be sufficient for the recall of the stored memories (Treves and Rolls, 1992), but recall from a noisy cue is suggested to trigger pattern separation (O'Reilly and McClelland, 1994). Therefore, solving ambiguity embedded in the blurred scenes

requires dentate gyrus which supports pattern separation, but solving ambiguity embedded in the masked scenes only requires intact CA3 recurrent connections and the perforant path inputs from the EC.

While the distinction between the blurred and masked scene stimuli are more clear, the difference between the blurred and overlay scenes seems more arbitrary. The degree of overlap with the original scenes could have affected whether the perforant path inputs can recruit the CA3 units. The relatively intact performance of DG-lesioned rats under mildly blurred conditions provides support for such an explanation (Fig. 5A). Computational models have also suggested that partial activity patterns in EC may not be sufficient for recruiting the original subset of the DG neurons (O'Reilly and McClelland, 1994). However, the group difference observed in highly blurred scene stimuli (Fig. 5A) suggests that the degree of changes in the EC needed for recruiting the original subset of DG neurons are relatively resilient to noise and more important factor could be whether competing subsets within the DG are recruited, such as in the Overlay sessions. Our results suggest that the DG is indispensable for this type of memory retrieval. Therefore, when environmental inputs are ambiguous, the mossy fiber-mediated inputs from the DG may carry some critical information for the CA3 network to access the original memory representations. Intact basic firing properties of CA3 cells in the DG-lesioned rats when retrieving relatively familiar visual scenes (Fig. 12) suggest that the DG network have more important role to play when environmental ambiguity exceeds a

certain threshold. Future studies should address the mechanism by which the DG network detects the level of ambiguity in the stimulus.

Consistent with the previous studies, there was some damage in the CA1 subfield as a result of the colchicine injection into the DG (Lee and Kesner, 2004; Jerman et al., 2005; Ahn and Lee, 2014). The degraded pattern separation of the single units in the CA3 in the DG-lesion group might be attributable to the partial damage in the CA1. However, prior behavioral studies reported dissociations in performance with similar colchicine-based lesion techniques and with a similar amount of damage in the CA1 (Gilbert et al., 2001; Lee and Kesner, 2003). Furthermore, the CA3 receives major inputs from the DG, CA3, or the entorhinal cortex, but not directly from the CA1 (Gonzales et al., 2001). Taken together, it is unlikely that the partial damage in the CA1 was the major cause of the degraded pattern separation in the DG-lesion group.

Another concern for the DG-lesion group is the absence of mossy cells in the hilar area in that group. Mossy cells in the hilar region may play key roles in providing feedback information to granule cells in the DG and bridging the CA3 and DG (Buckmaster et al., 1996). Inactivating mossy cells induced hyperactivity in granule cells and impaired pattern separation (Jinde et al., 2012). Unfortunately, because colchicine eliminates granule cells and mossy cells, it is impossible to determine the differential contributions of the different cell types in the current study. Future studies with more cell type-selective methods are required to address these issues.

How does the result of the current study fit the findings in recent electrophysiological studies on DG-CA3 circuitry? Despite using colchicine-induced DG lesion, we did not observe degraded spatial selectivity in CA3 units with DG lesion reported in a previous study (Sasaki et al., 2018). It is possible that the more complex nature of the radial arm maze used in their study could have triggered impaired spatial pattern separation between different arms and led to lower spatial selectivity. Also, there is a possibility that there are heterogeneous groups within the CA3 units with DG lesion since reduced spatial selectivity was only observed in the CA3 with the least mossy fiber input group in their study. Previous literature was divided on whether spatial firing patterns of the DG granule cells or CA3 pyramidal cells remain stable or remap when the external environment is changed (GoodSmith et al., 2017; Senzai and Buzsaki, 2017; van Dijk and Fenton, 2018). Results of the current study support that CA3 units remap by modulating its rate when different scenes are presented. The rate modulation observed in the current study could be driven by using two explicit scene stimuli, as compared to using an internal spatial reference frame(van Dijk and Fenton, 2018) or distal-local reference frames(GoodSmith et al., 2017).

One of the key findings in the current study is that, unlike blurring the scenes, the partial occlusion of the visual scene stimulus (*Masked* session) enabled rats perform the task without the DG and that CA3 cells exhibited pattern separation normally without the DG.

The neural mechanisms to explain why the DG is necessary only in recognizing the noisy stimuli (i.e., blurry scenes) but not for the partial stimuli (i.e., masked scenes) allow only speculations at this point. Although computational models assume that noisy and partial inputs might equally trigger pattern separation in the DG-CA3 networks (O'Reilly and McClelland, 1994), noisy inputs might necessitate the DG functions more than partial ones for pattern separation in the CA3. Another possibility is that the extra testing period during which rats experienced the blurred and overlaid stimuli might have allowed the CA3 network to develop a new way to conduct pattern separation (or pattern completion) without the DG. One may think of a possibility that rats might have dealt with the masked stimuli as objects and used the perirhinal cortex to solve the task without the DG. Although that might explain why the DG lesions did not result in performance deficits, it cannot explain how the CA3 network still exhibit pattern separation without the DG. Furthermore, our masks appeared at pseudo-random locations of the screen on different trials, making it difficult for the rat to see the same local patterns across different masked trials.

Recently, we have shown that neurons in the perirhinal cortex also exhibit pattern separator-like responses when rats were required to recognize ambiguously morphed images (Ahn and Lee, 2017). Although it would be ideal to record CA3 cells in the same object-recognition paradigm, several reasons make such an attempt difficult. First, in rodents, it is often difficult to use the touchscreen-based

recognition paradigm (Ahn and Lee, 2017) when physiologically recording neural activities from the hippocampus because principal neurons in the hippocampus are mostly place cells (especially in the dorsal hippocampus), meaning that they fire only when the animal is positioned within the place fields of those cells. The position-based firing properties of hippocampal cells make it very difficult to sample neural activities from enough cells when a behavioral apparatus requires the rat to perform the task in a fixed area. Second, unlike the results from the human studies (Kirwan and Stark, 2007; Bakker et al., 2008; Lacy et al., 2011; Motley and Kirwan, 2012; Stevenson et al., 2020), prior behavioral studies suggest that object recognition itself may not be hippocampal-dependent in rodents (Gilbert and Kesner, 2003; Jo and Lee, 2010). On the other hand, inactivating the perirhinal cortex in the current visual scene task resulted in only minor deficits (Park et al., 2017), compared to the devastating effects of the hippocampal inactivation (data not shown). Therefore, we reasoned that using a task that requires spatial navigation based on visual patterns that can be manipulated similarly as in the Ahn and Lee study for objects should provide the best experimental design to physiologically examine pattern separation in the CA3 with or without the DG. The results of the current study, together with our findings in the perirhinal cortex for object recognition (Ahn and Lee, 2017), strongly suggest that the neural networks perform the signature behavior of pattern separation across different regions of the brain when the optimal type of stimulus (e.g., objects in the

perirhinal cortex, visual scenes in the hippocampus) is ambiguously altered from the original pattern.

In the absence of the DG, cells in the CA3 tended to respond gradually to continuously changing ambiguous visual scenes. Inputs from the entorhinal cortex via the perforant path to the CA3 network are likely to scale linearly with the degree of stimulus similarity. The CA1 network also receives direct inputs from the entorhinal cortex, with prior studies showing the relatively linear mapping of environmental ambiguity by CA1 cells (Lee et al., 2004a; Leutgeb et al., 2004; Vazdarjanova and Guzowski, 2004). Our study confirms the nature of these entorhinal inputs to the hippocampus and reemphasizes the critical roles of the DG in implementing categorical dynamics in information processing using gradually changing inputs from the entorhinal cortex in the hippocampal network. Our findings suggest that the pattern-separating operations of the DG network may be necessary for the acquisition of novel environmental contexts as well as for the retrieval of memory representations when encountering altered environments. Such a pattern-separating computational component may be essential in orchestrating network dynamics to strategically organize behavior for efficient problem-solving in a goal-directed task.

Bibliography

Aggleton JP, Brown MW (1999) Episodic memory, amnesia, and the hippocampal-anterior thalamic axis. Behav Brain Sci 22:425-444; discussion 444-489.

Ahn JR, Lee I (2014) Intact CA3 in the Hippocampus is Only Sufficient for Contextual Behavior Based on Well-Learned and Unaltered Visual Background. Hippocampus 24:1081-1093.

Ahn JR, Lee I (2017) Neural Correlates of Both Perception and Memory for Objects in the Rodent Perirhinal Cortex. Cereb Cortex 27:3856-3868.

Amaral DG, Witter MP (1989) The three-dimensional organization of the hippocampal formation: a review of anatomical data. Neuroscience 31:571-591.

Amaral DG, Ishizuka N, Claiborne B (1990) Neurons, numbers and the hippocampal network. Prog Brain Res 83:1-11.

Amaral DG, Scharfman HE, Lavenex P (2007) The dentate gyrus: fundamental neuroanatomical organization (dentate gyrus for dummies). Prog Brain Res 163:3-22.

Andersen P, Bliss TV, Lomo T, Olsen LI, Skrede KK (1969) Lamellar organization of hippocampal excitatory pathways. Acta Physiol Scand 76:4A-5A.

Bakker A, Kirwan CB, Miller M, Stark CEL (2008) Pattern Separation in the Human Hippocampal CA3 and Dentate Gyrus. Science 319:1640-1642.

Barnes CA, McNaughton BL, Mizumori SJ, Leonard BW, Lin LH (1990) Comparison of spatial and temporal characteristics of neuronal activity in sequential stages of hippocampal processing. Prog Brain Res 83:287-300.

Berron D, Schutze H, Maass A, Cardenas-Blanco A, Kuijf HJ, Kumaran D, Duzel E (2016) Strong Evidence for Pattern Separation in Human Dentate Gyrus. J Neurosci 36:7569-7579.

Bonnici HM, Kumaran D, Chadwick MJ, Weiskopf N, Hassabis D, Maguire EA (2012) Decoding representations of scenes in the medial temporal lobes. Hippocampus 22:1143-1153.

Boss BD, Peterson GM, Cowan WM (1985) On the number of neurons in the dentate gyrus of the rat. Brain Res 338:144-150.

Brewer JB, Zhao Z, Desmond JE, Glover GH, Gabrieli JDE (1998) Making memories: Brain activity that predicts how well visual experience will be remembered. Science 281:1185-1187.

Brown TH, Johnston D (1983) Voltage-clamp analysis of mossy fiber synaptic input to hippocampal neurons. J Neurophysiol 50:487-507.

Brown TI, Hasselmo ME, Stern CE (2014) A high-resolution study of hippocampal and medial temporal lobe correlates of spatial context and prospective overlapping route memory. Hippocampus 24:819-839.

Brown TI, Ross RS, Keller JB, Hasselmo ME, Stern CE (2010) Which Way Was I Going? Contextual Retrieval Supports the Disambiguation of Well Learned Overlapping Navigational Routes. Journal of Neuroscience 30:7414-7422.

Buckmaster PS, Wenzel HJ, Kunkel DD, Schwartzkroin PA (1996) Axon arbors and synaptic connections of hippocampal mossy cells in the rat in vivo. J Comp Neurol 366:271-292.

Claiborne BJ, Amaral DG, Cowan WM (1986) A light and electron microscopic analysis of the mossy fibers of the rat dentate gyrus. J Comp Neurol 246:435-458.

Claiborne BJ, Amaral DG, Cowan WM (1990) Quantitative, three-dimensional analysis of granule cell dendrites in the rat dentate gyrus. J Comp Neurol 302:206-219.

Danielson NB, Turi GF, Ladow M, Chavlis S, Petrantonakis PC, Poirazi P, Losonczy A (2017) In Vivo Imaging of Dentate Gyrus Mossy Cells in Behaving Mice. Neuron 93:552-559 e554.

Davachi L, Mitchell JP, Wagner AD (2003) Multiple routes to memory: Distinct medial temporal lobe processes build item and source memories. Proceedings of the National Academy of Sciences of the United States of America 100:2157-2162.

de No RL (1934) Studies on the structure of the cerebral cortex XI Continuation of the study of the ammonic system. J Psychol Neurol 46:113-177.

Delcasso S, Huh N, Byeon JS, Lee J, Jung MW, Lee I (2014) Functional Relationships between the Hippocampus and Dorsomedial Striatum in Learning a Visual Scene-Based Memory Task in Rats. Journal of Neuroscience 34:15534-15547.

Dudchenko PA, Wood ER, Eichenbaum H (2000) Neurotoxic hippocampal lesions have no effect on odor span and little effect on odor recognition memory but produce significant impairments on spatial span, recognition, and alternation. Journal of Neuroscience 20:2964-2977.

Dupret D, O'Neill J, Pleydell-Bouverie B, Csicsvari J (2010) The reorganization and reactivation of hippocampal maps predict spatial memory performance. Nature neuroscience 13:995-1002.

Eacott MJ, Norman G (2004) Integrated memory for object, place, and context in rats: A possible model of episodic-like memory? Journal of Neuroscience

24:1948-1953.

Eichenbaum H (2000) A cortical-hippocampal system for declarative memory. Nat Rev Neurosci 1:41-50.

Eichenbaum H, Kuperstein M, Fagan A, Nagode J (1987) Cue-Sampling and Goal-Approach Correlates of Hippocampal Unit-Activity in Rats Performing an Odor-Discrimination Task. Journal of Neuroscience 7:716-732.

Felleman DJ, Van Essen DC (1991) Distributed hierarchical processing in the primate cerebral cortex. Cereb Cortex 1:1-47.

Fortin NJ, Wright SP, Eichenbaum H (2004) Recollection-like memory retrieval in rats is dependent on the hippocampus. Nature 431:188-191.

Gaffan D (1991) Spatial organization of episodic memory. Hippocampus 1:262-264.

Gaffan D (1994) Scene-specific memory for objects: a model of episodic memory impairment in monkeys with fornix transection. J Cogn Neurosci 6:305-320.

Gilbert PE, Kesner RP (2003) Recognition memory for complex visual discriminations is influenced by stimulus interference in rodents with perirhinal cortex damage. Learn Mem 10:525-530.

Gilbert PE, Kesner RP, DeCoteau WE (1998) Memory for spatial location: role of the hippocampus in mediating spatial pattern separation. J Neurosci 18:804-810.

Gilbert PE, Kesner RP, Lee I (2001) Dissociating hippocampal subregions: A double dissociation between dentate gyrus and CA1. Hippocampus 11:626-636.

Gonner L, Vitay J, Hamker FH (2017) Predictive Place-Cell Sequences for Goal-

Finding Emerge from Goal Memory and the Cognitive Map: A Computational Model. Front Comput Neurosci 11:84.

Gonzales RB, DeLeon Galvan CJ, Rangel YM, Claiborne BJ (2001) Distribution of thorny excrescences on CA3 pyramidal neurons in the rat hippocampus. J Comp Neurol 430:357-368.

GoodSmith D, Chen X, Wang C, Kim SH, Song H, Burgalossi A, Christian KM, Knierim JJ (2017) Spatial Representations of Granule Cells and Mossy Cells of the Dentate Gyrus. Neuron 93:677-690 e675.

Hassabis D, Kumaran D, Vann SD, Maguire EA (2007) Patients with hippocampal amnesia cannot imagine new experiences. Proceedings of the National Academy of Sciences of the United States of America 104:1726-1731.

Henderson JM, Hollingworth A (1999) High-level scene perception. Annu Rev Psychol 50:243-271.

Hok V, Lenck-Santini PP, Roux S, Save E, Muller RU, Poucet B (2007) Goal-related activity in hippocampal place cells. Journal of Neuroscience 27:472-482.

Hollup SA, Molden S, Donnett JG, Moser MB, Moser EI (2001) Accumulation of hippocampal place fields at the goal location in an annular watermaze task. Journal of Neuroscience 21:1635-1644.

Jadhav SP, Rothschild G, Roumis DK, Frank LM (2016) Coordinated Excitation and Inhibition of Prefrontal Ensembles during Awake Hippocampal Sharp-Wave Ripple Events. Neuron 90:113-127.

Jerman TS, Kesner RP, Lee I, Berman RF (2005) Patterns of hippocampal cell loss based on subregional lesions of the hippocampus. Brain Res 1065:1-7.

Jinde S, Zsiros V, Jiang Z, Nakao K, Pickel J, Kohno K, Belforte JE, Nakazawa K

(2012) Hilar mossy cell degeneration causes transient dentate granule cell hyperexcitability and impaired pattern separation. Neuron 76:1189-1200.

Jo YS, Lee I (2010) Disconnection of the hippocampal-perirhinal cortical circuits severely disrupts object-place paired associative memory. J Neurosci 30:9850-9858.

Kim S, Lee J, Lee I (2012) The hippocampus is required for visually cued contextual response selection, but not for visual discrimination of contexts. Frontiers in behavioral neuroscience 6:66.

Kirwan CB, Stark CE (2007) Overcoming interference: an fMRI investigation of pattern separation in the medial temporal lobe. Learn Mem 14:625-633.

Kirwan CB, Wixted JT, Squire LR (2008) Activity in the medial temporal lobe predicts memory strength, whereas activity in the prefrontal cortex predicts recollection. J Neurosci 28:10541-10548.

Kobayashi T, Nishijo H, Fukuda M, Bures J, Ono T (1997) Task-dependent representations in rat hippocampal place neurons. J Neurophysiol 78:597-613.

Lacy JW, Yassa MA, Stark SM, Muftuler LT, Stark CE (2011) Distinct pattern separation related transfer functions in human CA3/dentate and CA1 revealed using high-resolution fMRI and variable mnemonic similarity. Learn Mem 18:15-18.

Lee H, Wang C, Deshmukh SS, Knierim JJ (2015) Neural Population Evidence of Functional Heterogeneity along the CA3 Transverse Axis: Pattern Completion versus Pattern Separation. Neuron 87:1093-1105.

Lee I, Kesner RP (2003) Differential roles of dorsal hippocampal subregions in spatial working memory with short versus intermediate delay. Behav

Neurosci 117:1044-1053.

Lee I, Kesner RP (2004) Encoding versus retrieval of spatial memory: double dissociation between the dentate gyrus and the perforant path inputs into CA3 in the dorsal hippocampus. Hippocampus 14:66-76.

Lee I, Solivan F (2010) Dentate gyrus is necessary for disambiguating similar object-place representations. Learning and Memory 17:252-258.

Lee I, Kim J, Lee C (1999) Anatomical characteristics and three-dimensional model of the dog dorsal lateral geniculate body. Anat Rec JID - 0370540 256:29-39.

Lee I, Rao G, Knierim JJ (2004a) A double dissociation between hippocampal subfields: differential time course of CA3 and CA1 place cells for processing changed environments. Neuron 42:803-815.

Lee I, Yoganarasimha D, Rao G, Knierim JJ (2004b) Comparison of population coherence of place cells in hippocampal subfields CA1 and CA3. Nature 430:456-459.

Lee I, Griffin AL, Zilli EA, Eichenbaum H, Hasselmo ME (2006) Gradual translocation of spatial correlates of neuronal firing in the hippocampus toward prospective reward locations. Neuron 51:639-650.

Lee J, Yun M, Cho E, Lee JW, Lee D, Jung MW (2019) Transient effect of mossy fiber stimulation on spatial firing of CA3 neurons. Hippocampus 29:639-651.

Lee KJ, Park SB, Lee I (2014) Elemental or contextual? It depends: individual difference in the hippocampal dependence of associative learning for a simple sensory stimulus. Frontiers in behavioral neuroscience 8:217.

Leutgeb JK, Leutgeb S, Moser M-B, Moser EI (2007) Pattern Separation in the

Dentate Gyrus and CA3 of the Hippocampus. Science 315:961-966.

Leutgeb S, Leutgeb JK, Treves A, Moser MB, Moser EI (2004) Distinct ensemble codes in hippocampal areas CA3 and CA1. Science 305:1295-1298.

Marr D (1971) Simple memory: a theory for archicortex. Philosophical transactions of the Royal Society of London Series B, Biological sciences 262:23-81.

McKenzie S, Robinson NTM, Herrera L, Churchill JC, Eichenbaum H (2013) Learning Causes Reorganization of Neuronal Firing Patterns to Represent Related Experiences within a Hippocampal Schema. Journal of Neuroscience 33:10243-10256.

McNaughton BL, Barnes CA, Meltzer J, Sutherland RJ (1989) Hippocampal granule cells are necessary for normal spatial learning but not for spatially-selective pyramidal cell discharge. Exp Brain Res 76:485-496.

Motley SE, Kirwan CB (2012) A parametric investigation of pattern separation processes in the medial temporal lobe. J Neurosci 32:13076-13085.

Mu Y, Zhao C, Gage FH (2011) Dopaminergic modulation of cortical inputs during maturation of adult-born dentate granule cells. J Neurosci 31:4113-4123.

Mullally SL, Vargha-Khadem F, Maguire EA (2014) Scene construction in developmental amnesia: An fMRI study. Neuropsychologia 52:1-10.

Muller RU, Kubie JL (1987) The effects of changes in the environment on the spatial firing of hippocampal complex-spike cells. J Neurosci 7:1951-1968.

Murray EA, Mishkin M (1998) Object recognition and location memory in monkeys with excitotoxic lesions of the amygdala and hippocampus. Journal of Neuroscience 18:6568-6582.

Nakashiba T, Cushman JD, Pelkey KA, Renaudineau S, Buhl DL, McHugh TJ, Rodriguez Barrera V, Chittajallu R, Iwamoto KS, McBain CJ, Fanselow

MS, Tonegawa S (2012) Young dentate granule cells mediate pattern separation, whereas old granule cells facilitate pattern completion. Cell 149:188-201.

Nakazawa K (2017) Dentate Mossy Cell and Pattern Separation. Neuron 93:1236.

Neunuebel JP, Knierim JJ (2014) CA3 Retrieves Coherent Representations from Degraded Input: Direct Evidence for CA3 Pattern Completion and Dentate Gyrus Pattern Separation. Neuron 81:416-427.

O'Keefe J, Dostrovsky J (1971) The hippocampus as a spatial map. Preliminary evidence from unit activity in the freely-moving rat. Brain Res 34:171-175.

O'Keefe J, Conway DH (1978) Hippocampal place units in the freely moving rat: why they fire where they fire. Exp Brain Res 31:573-590.

O'Keefe J, Nadel L (1978) The hippocampus as a cognitive map. Oxford: Clarendon Press.

O'Reilly RC, McClelland JL (1994) Hippocampal conjunctive encoding, storage, and recall: avoiding a trade-off. Hippocampus 4:661-682.

Park EH, Ahn JR, Lee I (2017) Interactions between stimulus and response types are more strongly represented in the entorhinal cortex than in its upstream regions in rats. eLife 6.

Ramón y Cajal S (1893) Estructura del asta de Ammon y fascia dentata. Madrid: Tip. de Fortanet.

Rolls ET, Kesner RP (2006) A computational theory of hippocampal function, and empirical tests of the theory. Prog Neurobiol 79:1-48.

Rolls ET, Kesner RP (2016) Pattern separation and pattern completion in the hippocampal system. Introduction to the Special Issue. Neurobiol Learn Mem 129:1-3.

Sakon JJ, Suzuki WA (2019) A neural signature of pattern separation in the monkey hippocampus. ProcNatlAcadSciUSA 116:9634-9643.

Sasaki T, Piatti VC, Hwaun E, Ahmadi S, Lisman JE, Leutgeb S, Leutgeb JK (2018) Dentate network activity is necessary for spatial working memory by supporting CA3 sharp-wave ripple generation and prospective firing of CA3 neurons. Nature neuroscience 21:258-269.

Schwarz G (1978) Estimating the Dimension of a Model. The Annals of Statistics 6:461-464.

Scoville WB, Milner B (1957) Loss of recent memory after bilateral hippocampal lesions. JNeurolNeurosurgPsychiatry 20:11-21.

Senzai Y, Buzsaki G (2017) Physiological Properties and Behavioral Correlates of Hippocampal Granule Cells and Mossy Cells. Neuron 93:691-704 e695.

Skaggs WE, McNaughton BL, Gothard KM (1993) An information-theoretic approach to deciphering the hippocampal code. In: Advances in neural information processing systems, pp 1030-1037.

Squire LR, Zola-Morgan S (1991) The medial temporal lobe memory system. Science 253:1380-1386.

Stark CE, Okado Y (2003) Making memories without trying: medial temporal lobe activity associated with incidental memory formation during recognition. J Neurosci 23:6748-6753.

Stevenson RF, Reagh ZM, Chun AP, Murray EA, Yassa MA (2020) Pattern Separation and Source Memory Engage Distinct Hippocampal and Neocortical Regions during Retrieval. J Neurosci 40:843-851.

Treves A, Rolls ET (1992) Computational constraints suggest the need for two distinct input systems to the hippocampal CA3 network. Hippocampus

2:189-199.

Treves A, Rolls ET (1994) Computational analysis of the role of the hippocampus in memory. Hippocampus 4:374-391.

Tulving E, Donaldson W, Bower GH, United States. Office of Naval Research. (1972) Organization of memory. New York,: Academic Press.

van Dijk MT, Fenton AA (2018) On How the Dentate Gyrus Contributes to Memory Discrimination. Neuron 98:832-+.

Vazdarjanova A, Guzowski JF (2004) Differences in hippocampal neuronal population responses to modifications of an environmental context: evidence for distinct, yet complementary, functions of CA3 and CA1 ensembles. J Neurosci 24:6489-6496.

Walsh TJ, Schulz DW, Tilson HA, Schmechel DE (1986) Colchicine-induced granule cell loss in rat hippocampus: selective behavioral and histological alterations. Brain Res 398:23-36.

Wang Z, Bovik AC, Sheikh HR, Simoncelli EP (2004) Image quality assessment: from error visibility to structural similarity. IEEE Trans Image Process 13:600-612.

Wood ER, Dudchenko PA, Robitsek RJ, Eichenbaum H (2000) Hippocampal neurons encode information about different types of memory episodes occurring in the same location. Neuron 27:623-633.

Xavier GF, Oliveira-Filho FJ, Santos AM (1999) Dentate gyrus-selective colchicine lesion and disruption of performance in spatial tasks: difficulties in "place strategy" because of a lack of flexibility in the use of environmental cues? Hippocampus 9:668-681.

Zeidman P, Mullally SL, Maguire EA (2015) Constructing, Perceiving, and

Maintaining Scenes: Hippocampal Activity and Connectivity. Cereb Cortex 25:3836-3855.

Acknowledgement (감사의 말)

이 논문을 집필하기까지 지도해주신 이인아 교수님께 감사를 드립니다. 첫 논문에서 사람을 대상으로 뇌 영상 연구를 한 제가 새로운 영역인 전기 생리학 연구를 진행하는 과정에서 교수님의 많은 지지와 격려로 인해 연구를 시작할 수 있었고, 연구를 진행하는 과정에서도 여러 번 실패와 낙담을 경험하였지만 교수님의 지도 덕분에 의미 있는 연구 결과를 맺을 수 있었습니다.

본 연구를 진행하는 과정에서 항상 힘이 되어준 연구실 동료들께 감사드립니다. 실험과 관련되어 많은 도움을 주었던 요섭이, 성하 형, 전기 생리학 자료 분석에 도움을 주었던 현우, 성범, 수민, 진승우에게도 특별히 감사를 표하고 싶습니다. 그리고, 쥐 수술을 배워가면서 많은 것을 알려주었고, 대학원 기간동안 정말 많은 격려를 해준 재롱이형과 유승우에게도 감사의 말을 전하고 싶습니다. 논문을 집필하는 과정에서 집중할 수 있도록 배려해준 보나와 재민이에게도 감사를 표합니다. 또한, 좋은 연구실 동료로써 연구에 도움을 주었던 은혜, 흥열, 혜리, 희승, 소희, 승배, 수빈이에게도 감사를 전하고 싶습니다.

학위 과정 중에 끊임없는 지원와 기도로 도움을 준 제 가족들이 있었기에 그 모든 과정을 이겨낼 수 있었던 것 같습니다. 사랑하는 아버지, 어머지, 그리고 형, 형수님, 지온이와 정인이에게 많은 응원을 받아 그 고마움을 표하고 싶습니다. 마지막으로 제 삶을 주관하시는 하나님께 감사 드립니다.

국문초록

치상회 손상에 따른 CA3 장소세포의 장면의존적 발화율 변조의 저하

이충희

특정 환경에 적합한 행동을 하기 위해 우리는 과거에 그 환경에서 어떠한 경험을 하였는지 반추한다. 해마는 이와 같이 과거에 경험한 사건 등에 대한 일화 기억을 처리할 때 중요한 뇌 영역이라고 알려져 있다. 항상 변화하는 환경 속에서 매번 과거와 동일한 자극을 경험하긴 어렵다. 따라서, 일화 기억의 처리에는 서로 유사하지만 다른 상황을 구분하는 과정이 필요하다. 해마의 하위 영역인 치상회는 서로 유사한 자극을 분리하여 저장하기 위해 필요하다고 알려져 있으나, 단위신경세포 수준의 정보처리 기전은 아직 알려진 바 없다.

이 논문에서는 최근 일화 기억의 저장과 인출 과정이 시각적으로 들어오는 장면에 대한 처리와 밀접한 연관을 가지고 있다는 주장에 기반하여, 유사한 장면 자극들이 해마에서 처리되는 기전에 대한 연구를 진행하였다. 이 연구에서는 콜치신을 사용한 쥐의 치상회의 손상이 시각 장면 기억 과제의 수행을 저해하는지 그 행동적 영향을 검증하였다. 또한, 치상회로부터 정보를 받는 CA3영역의 단위신경세포의 활동 전위가 어떠한 방식으로 장면 자극을 표상하고, 기존에 학습했던 장면 자극이 변형되었을 때는 어떻게 표상하는지, 그리고 그 표상 방식들이 치상회의 손상 여부에 따라 어떻게 영향을 받는지 전기생리학적 검증을 시도하였다.

통제 집단에 비해 치상회 손상 집단은 기존에 학습하였던 장면 자극이 흐릿하게 제시될 때에만 낮은 과제 수행률을 보였다. 동시에 치상회가 손상된 쥐들의 CA3 단위신경세포의 시각 장면 관련 발화율 변조가 흐릿한 장면 자극이 제시되었을 때 현저하게 감소하였다. 이는 치상회가 손상된 쥐의 CA3 단위신경세포가 통제 집단에 비해 흐릿한 장면 자극의 모호성의 정도에 따른 범주적 변화를 보여주지 않았기 때문이다. 본 연구는 치상회가 CA3 영역이 애매한 장면에 직교적으로 반응하게 함으로써 장면 기억을 저장하는 과정뿐만 아니라, CA3와 함께 수정된 시각 장면이 처리될 때에도 핵심적인 역할을 한다는 것을 규명하였다.